Statistical-Empirical Modelling of Airfoil Noise Subjected to Leading Edge Serrations

Till M. Biedermann[1]
ISAVE, Duesseldorf University of Applied Sciences, Duesseldorf, D-40474, Germany

Tze Pei Chong[2]
Department of Mechanical, Aerospace and Civil Engineering, Brunel University London, Uxbridge, UB8 3PH, United Kingdom

Frank Kameier[3]
ISAVE, Duesseldorf University of Applied Sciences, Duesseldorf, D-40474, Germany

and
Christian O. Paschereit[4]
Berlin Technical University, Berlin, D-10623, Germany

With the objective of reducing the broadband noise from the interaction of highly turbulent flow and airfoil leading edge, sinusoidal leading edge serrations were investigated as an effective passive treatment. An extensive aeroacoustic study was performed in order to determine the main influences and interdependencies of factors, such as the Reynolds number, turbulence intensity, serration amplitude and wavelength as well as the angle of attack on the noise reduction capability. A statistical-empirical model was developed to predict the overall sound pressure level and noise reduction of a NACA65(12)-10 airfoil with and without leading edge serrations in the range of chord-based Reynolds numbers of $2.5 \cdot 10^5 \leq Re \leq 6 \cdot 10^5$. The observed main influencing factors on the noise radiation were quantified in a systematic order for the first time. Moreover, significant interdependencies of the turbulence intensity and the serration wavelength, as well as the serration wavelength and the angle of attack were observed, validated and quantified. The statistical-empirical model was validated against an external set of experimental data, which is shown to be accurate and reliable.

[1] Doctoral Researcher, Institute of Sound and Vibration Engineering *ISAVE*, till.biedermann@hs-duesseldorf.de, AIAA Student Member
[2] Senior Lecturer, Department of Mechanical, Aerospace and Civil Eng., t.p.chong@brunel.ac.uk, AIAA Member
[3] Professor, Institute of Sound and Vibration Engineering *ISAVE*, frank.kameie@hs-duesseldorf.de
[4] Professor, Institute of Fluid Dynamics and Technical Acoustics *ISTA*, oliver.paschereit@tu-berlin.de

Nomenclature

A	=	*amplitude of leading edge serrations [mm]*
λ	=	*wavelength of leading edge serrations [mm]*
U_0	=	*free stream velocity [ms^{-1}]*
ρ_0	=	*fluid density [kgm^{-3}]*
c	=	*sound velocity[ms^{-1}]*
Tu	=	*turbulence intensity [%]*
Re	=	*chord-based Reynolds number [--]*
C	=	*airfoil chord length [mm]*
S	=	*airfoil span [mm]*
H	=	*nozzle height [mm]*
R	=	*observer distance in the far-field [m]*
d	=	*maximum airfoil thickness [mm]*
AoA	=	*angle of attack [°], equals non-dimensional vertical displacement z/H*
x	=	*local streamwise (longitudinal) coordinate [mm]*
y	=	*local anti-streamwise (transversal) coordinate [mm]*
z	=	*local vertical coordinate [mm]*
$OASPL$	=	*overall sound pressure level [dB]*
$\Delta OASPL$	=	*overall sound pressure level reduction [dB]*
SPL	=	*sound pressure level [dB]*
ΔSPL	=	*sound pressure level reduction [dB]*
f	=	*frequency [Hz]*
ω	=	*angular frequency [s^{-1}]*
Θ	=	*polar angle [deg]*
Ma	=	*Mach number [--]*
LE	=	*leading edge*

I. Introduction

RECENT research has firmly established sinusoidal leading edge (*LE*) serrations as an effective passive treatment to reduce the broadband noise of an airfoil when exposed to a highly turbulent flow. A reduction in the overall sound pressure level of up to $\Delta OASPL = 7$ dB and the sound pressure level reductions $\Delta SPL > 10$ dB in the relevant frequency region could be achieved [1–4]. Although different hypotheses on the noise reduction mechanism were proposed before, they have hitherto not been comprehensively verified. In general, three mechanisms could be responsible for the reduction in the broadband noise. First is the reduced spanwise correlation coefficients as a result of incoherent response times of the incoming turbulence; second, a reduction of the acoustic sources as manifested in the reduction in pressure fluctuation at the serration peak; and third, a reduction of the streamwise turbulence intensity due to the converging flow within the serration gaps [5, 6].

Up to now, research on the effect of *LE* serrations focused either on the noise reduction capability, or on the aerodynamic performance of the airfoil itself. The effect of sinusoidal *LE* on the lift and drag forces has been analyzed experimentally, numerically and through the use of flow pattern visualization [7, 8]. Moreover, a numerical study to optimize the serration design in order to improve the aerodynamic forces on the airfoil was presented [9]. Of particular importance is the correlation between the aerodynamic flow behaviors and aeroacoustic noise reduction mechanisms. In general, the incoming turbulence amplifies the surface pressure fluctuations close to the airfoil *LE*, which then radiate into broadband noise [10, 11].

Recently, there have been many studies using high-fidelity numerical flow simulation to provide a physical insight of the noise reduction mechanisms by the serration [12–14]. These studies show that the surface pressure fluctuation and the far field noise on a serrated leading edge are de-correlated by the serrated *LE*s. In particular, the noise source at the mid-region of the oblique edge becomes ineffective across the mid to high frequency range. The serration could cause a significant decrease in the surface pressure fluctuations around the tip and mid-regions of the serration and subsequently reduce the broadband noise level. Another noise reduction mechanism is attributed to the phase interference and destruction effect between the serration peak and the mid-region of the oblique edge. Accordingly, the serration root could still remain effective in the noise radiation. Interestingly, a small modification of the serration root has been found to be able to further reduce the *LE* noise level [15]. The converging nature of the serration could also generate a nozzle effect to accelerate the flow within and reduce the level of turbulence intensity before the fluid-structure interaction near the stagnation points. Analytical work also begins to emerge that

generalizes Amiet's theory of leading edge noise to calculate the airfoil response function subjected to serrated *LE*s of different serration wavelengths and amplitudes and the far field noise radiation [16]. Although the analytical model can predict the acoustic power spectral densities that match reasonably well with the experimental results [1], the requirement of the iterative solving procedure to calculate the gust response function of the appropriate order makes it not straightforward to use. This paper aims to generalize the airfoil noise subjected to *LE* serrations by developing a statistical–empirical model.

Several parameters have been found to influence the effectiveness of noise reduction by *LE* serrations, which include the Reynolds number (*Re*), turbulence intensity (*Tu*), serration amplitude (*A/C*), serration wavelength (λ/C) and angle of attack (*AoA*). However, up to now, these parameters have been investigated independently, and only little effort was made to analyze them as an interrelated system of factors with respect to the noise reduction. This serves as motivation for the current work, where a comprehensive statistical–empirical model has been developed with the aim to describe the noise radiation of serrated *LEs* as an interrelated system involving the aforementioned five influencing parameters. Note that the current model does not predict the acoustic spectral characteristics for individual airfoil of serrated leading edges. Rather, the target value describing the noise radiation and noise reduction by the *LE* serrations is defined as the Overall Sound Pressure Level (*OASPL*).

II. Experimental Setup

In the current study, a cambered NACA65(12)-10 airfoil was chosen due to its relevance in the real-life application such as the stator vanes or axial fan blades. As shown in Fig. 1, the airfoil has a chord length of C = 150 mm and a span width of S = 300 mm. The airfoil geometry consists a removable frontal part ($0 < x/C < 0.3$) that allows various *LE* serration profiles to be attached. Once attached to the rear part main body, the serrations give the appearance that they are cut into the airfoil's main body. Therefore the maximum chord is always held constant at C = 150 mm for all the configurations [2]. The serration geometries are predominantly defined by their amplitude (chordwise peak-to-trough value) and wavelength (spanwise peak-to-peak-value). Both parameters would be normalized by the airfoil chord length throughout the paper. The shape of the *LE* serrations is designed according to a sinusoidal curve, and the NACA65(12)-10 profile was extruded along the line of this curve. An important feature of the current design is the semi-cyclic shape of the serration tips as depicted in Fig. 1.

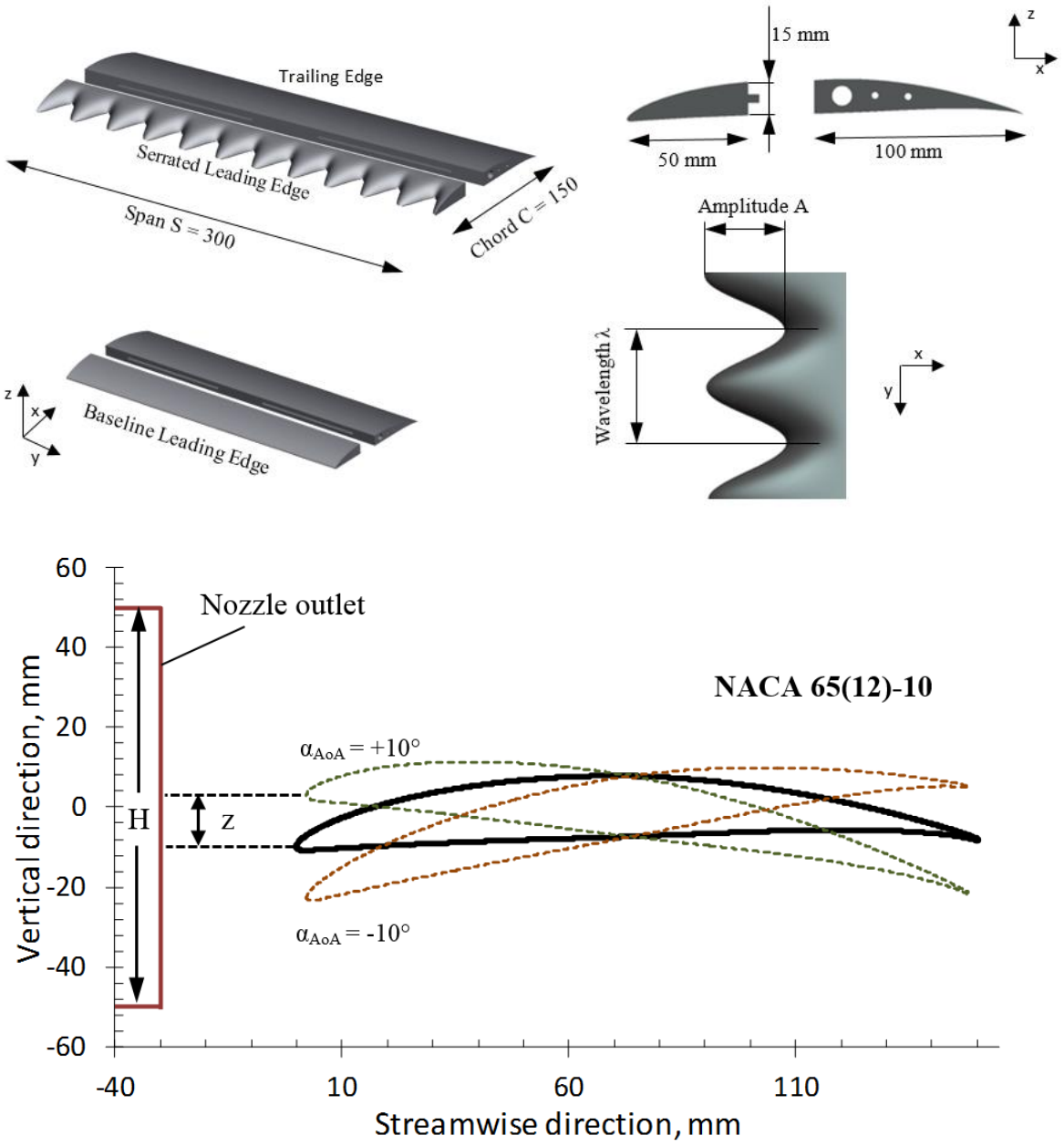

Fig. 1 NACA65(12)-10 airfoil showing the main body, the re-attachable leading edges and the definition and dimension of the various geometrical parameters.

The angle of attack, α refers to the geometrical angle between the horizontal axis and the chord line of the NACA65(12)-10 airfoil. As shown in Fig. 1, the non-dimensional ratio between the vertical *LE* tip displacement (z) and the height of the nozzle outlet (H) is also equivalent to the α. As shown in Table 1, an experimental investigation into the aerodynamic performance of the airfoil with a baseline *LE* in a closed-wind tunnel produces a

lift coefficient, C_L = 0.64 at α = 0°. The airfoil was attached to the side-plates extending from both sides of the nozzle outlet.

A pivot-mounted insert of the side-plates facilitates accurate rotation of the airfoil between $\alpha = \pm 10^o$. Due to the relatively low value of H in the current nozzle, measurement beyond $\alpha = \pm 10^o$ was not attempted. Note that no correction of the free jet deflection was applied in the current study. Therefore, it is more effective to use the non-dimensional quantity of z/H to represent the angle-alignment between the incoming mean flow and the airfoil leading edge instead of the geometrical angle α.

Table 1 Coefficients of lift, drag and lift-to-drag ratio at z/H = 0 and Re = 250,000. Measurements took place at the closed wind tunnel at Brunel University London.

	A/C	λ/C	C_L	C_D	C_L/C_D
BSLN	--	--	0.637	0.0342	18.62
A29λ26	*0.19*	*0.17*	0.550	0.0336	16.37
A22λ18	*0.12*	*0.12*	0.540	0.0338	15.95
A35λ18	*0.23*	*0.12*	0.566	0.0356	15.91
A22λ34	*0.12*	*0.23*	0.521	0.0330	15.79
A35λ34	*0.23*	*0.23*	0.564	0.0325	17.36
A12λ26	*0.08*	*0.17*	0.539	0.0335	16.06
A45λ26	*0.30*	*0.17*	0.497	0.0330	15.07
A29λ7.5	*0.19*	*0.05*	0.478	0.0363	13.16
A29λ45	*0.19*	*0.30*	0.586	0.0309	18.97

The noise experiments took place at the open jet wind tunnel of the aeroacoustic facility at Brunel University London. The exit nozzle, which has a dimension of 100 mm x 300 mm, is situated inside a semi-anechoic chamber (4.0 m x 5.0 m x 3.4 m). It can produce a typical turbulence intensity of between 0.1 % and 0.2 % [17, 2]. The maximum jet velocity is about 80 ms^{-1}. In order to generate elevated turbulence intensities (Tu) at the freestream, several turbulence grids of different mesh size (M) and bar diameter (d) were used. As per the criteria suggested by Laws and Livesey [18], all the turbulence grids are biplane square meshes with a constant ratio between the mesh size and the bar diameter (M/d = 5). Using the turbulence prediction model by Aufderheide et al. [19], which is based on the work of Laws and Livesey [18], five different turbulence grids that were predicted to generate Tu in the range of 2.1% and 5.5% were manufactured. The integral length scale of the turbulent eddies was found to be a function of Tu, but it was not included as a parameter to be investigated in the current noise modelling analysis.

In order to determine the Tu, a 1-D hot wire probe was placed at 30 mm downstream of the nozzle exit, which coincides with the airfoil leading edge tip when installed. The Tu was measured without a mounted airfoil, but with

the turbulence grids and side-plates installed. The mean velocity U_0 and *Tu* profiles were recorded at 106 locations over the whole nozzle exit area.

The velocity range of investigation was 10 $ms^{-1} \leq U_0 \leq 60$ ms^{-1} in steps of $\Delta U_0 = 10$ ms^{-1}. All measurements were repeated once to reduce the statistical spread and to reduce the uncertainty. After ensuring a uniform turbulence distribution in the measurement plane, the *Tu* for the present study was determined as the average value across the plane. The distance of the airfoil's leading edge to the nozzle exit remains the same for all the turbulence grids. The turbulence level near the airfoil's *LE* will be shown to be isotropic. Figure 2 demonstrates that the measured turbulent energy spectra of the fluctuating velocity agree well with the turbulence model of von Kármán and Liepmann for longitudinal isotropic turbulence as per the Eq. (1). The correction function of Rozenberg [20] in Eq. (2) was applied to the turbulence model in order to correct the turbulent energy in the high-frequency region close to the Kolmogorov scale. $\overline{u'^2}$ is the velocity fluctuation, Λ_{uu} is the integral length scale, K_x is the streamwise wave number and K_η is a parameter that controls the slope of the high-frequency roll-off. The range of chord-based Reynolds number investigated in this study is $2.5\text{x}10^5 \leq Re \leq 6\text{x}10^5$. The lower limit of the Reynolds number was determined by the minimum freestream velocity where isotropic condition of the *Tu* can still be established.

$$\Phi_{uu}^{L}(\omega) = \frac{\overline{u'^2}\Lambda_{uu}}{\pi U_0} \cdot \frac{1}{1+K_x^2\Lambda_{uu}^{\ 2}} \tag{1}$$

$$G_{Kolm.} = exp\left(\left(-9/4\right) \cdot \left(K_x/K_\eta\right)^2\right) \tag{2}$$

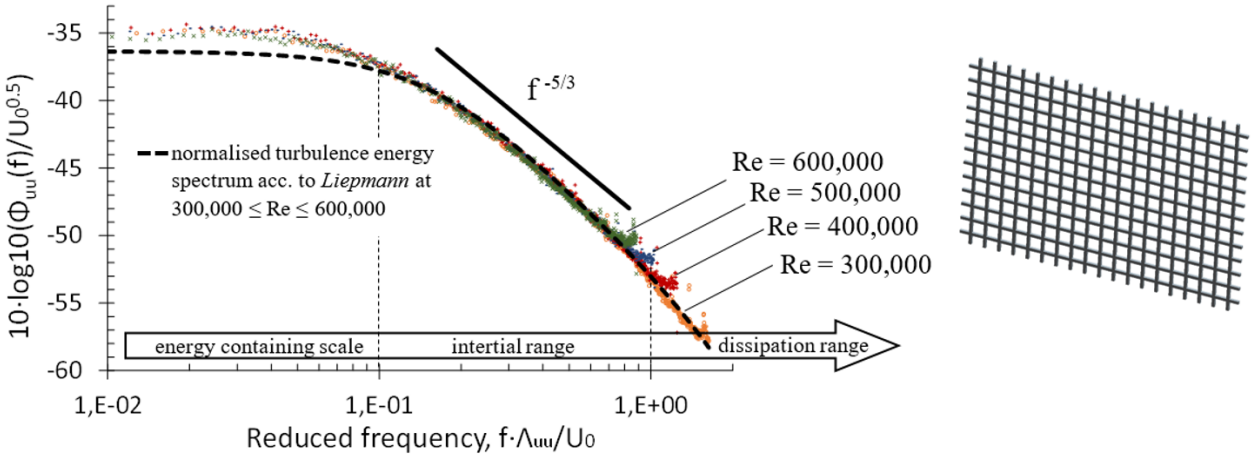

Fig. 2 Comparison of the normalized turbulence energy spectra between the theory (*Liepmann*) and experiment at 300,000 ≤ *Re* ≤ 600,000 and *Tu* = 3.9%. The streamwise location of the measurement coincides with the airfoil leading edge.

A statistical-empirical model describing the acoustic response, as a function of five influencing parameters, will be presented in Section IV. Because of the parameters chosen for the Design of Experiments (*DoE*), which will be discussed in Section III, a total of ten *LE* sections were investigated. These include one configuration with a straight *LE* to serve as the baseline case (*BSLN*). To conduct free field measurements of the *AGI*-Noise (Airfoil-Gust-Interaction), the airfoil was held by side-plates to keep the airfoil in place and to keep a two-dimensional flow profile [2]. Noise measurements at the aeroacoustic wind tunnel were made by a single PCB ½-inch prepolarised ICP® condenser microphone at polar angles of $\Theta = 90$ degree at a vertical distance of 0.95 m from the *LE* of the airfoil at mid-span (Fig. 3). The acoustic data was recorded at a sampling rate of 40 kHz, where the measurement time was set to 20 s. In the spectral analysis Hamming windows were used for windowing at 50% overlap by using a block size of 1024, yielding a frequency resolution of $\Delta f = 43$ Hz and resulting in a number of 1718 averaged blocks for the generated spectra. All the power spectral density (*PSD*) presented in this study has a 1 Hz frequency bandwidth.

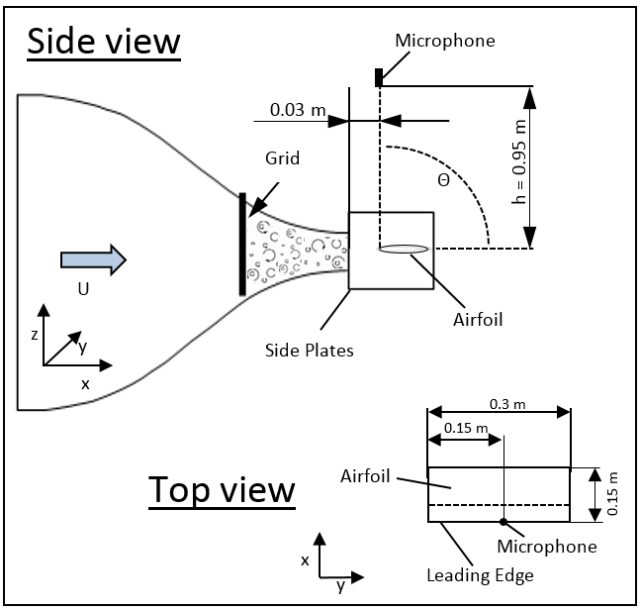

Fig. 3 Schematic of the experimental setup.

The frequency range ($f_1 \leq f \leq f_2$) chosen for the analysis in the Overall Sound Pressure Level (*OASPL*) is set to f_1 = 300 Hz and f_2 = 10 kHz. The decision on f_1 is due to the consideration of the cut-off frequency of the anechoic chamber. The f_2 is decided upon the exclusion of the possible influences by the airfoil self-noise from the trailing edge, which is not related to *AGI* noise. It is known that the *OASPL* could be very sensitive to the choice of f_1.

A careful sensitivity study was performed to examine the change in *OASPL* and Δ*OASPL* with regard to the different values of f_1. The sensitivity study demonstrates that both the *OASPL* and Δ*OASPL* are reasonably unaffected at $f_1 \geq 200$ Hz. Therefore, the current choice of f_1 = 300 Hz should be able to characterize the *AGI* noise accurately in the *OASPL* analysis. Another sensitivity study was also performed to the statistical model, which also confirms that the most dominant parameters will remain unaffected as long as $f_1 \geq 200$ Hz.

Table 2 Non-dimensional *DoE* (Design of Experiments) levels of the different factors of interest.

	Unit	**$-\alpha_{DoE}$**	**-1_{DoE}**	**0_{DoE}**	**$+1_{DoE}$**	**$+\alpha_{DoE}$**
x_{Nondim}	--	*-2.378*	*-1.0*	*0.0*	*+1.0*	*+2.378*
Re	--	250,000	351,422	425,000	498,578	600,000
Tu(u)	%	2.08	3.07	3.79	4.51	5.50
A_{Serr}/C	--	0.080	0.144	0.190	0.236	0.300
λ_{Serr}/C	--	0.050	0.122	0.175	0.228	0.300
z/H	--	-0.128	-0.054	0.000	0.054	0.128

A. Measurement Environment

The range of jet speeds under investigation is 25 $ms^{-1} \leq U_o \leq$ 60 ms^{-1}, corresponding to Reynolds' numbers based on the airfoil chord length of $2x5 \cdot 10^5 \leq Re \leq 6x10^5$, respectively. As shown in Table 2, the minima and maxima correspond to each of the five influencing parameters are defined. Preliminary measurements were performed at the extreme flow conditions prior to the main acoustic study to ensure that the background noise of the wind tunnel facility is well below the *AGI*-Noise. At the minimum and maximum fan speed, the acoustic spectra of the background noise, the baseline airfoil and the airfoil with the A45λ7.5 serrated *LE* (expected to produce the largest reduction in the *AGI*-noise level [2]) were measured. The acoustic results are shown in Fig. 4. The angle of attack was chosen to be at zero degree, and the *Tu* at the vicinity of the *LE* is at the maximum of 5.5%. The narrow band spectra in Fig. 4 demonstrate that the background noise without the presence of an airfoil in the free jet, but still with both the turbulence grid and side-plates, produces a significant lower sound pressure level compared to the cases when the airfoil is present. Moreover, the sound pressure level in the case of the airfoil with a serrated *LE* (*A*45λ7.5 case) is always above the background noise, especially in the intermediate frequency region of interest between 300 Hz and 5 kHz, where the main contribution of the noise reduction is expected to come from the serrations.

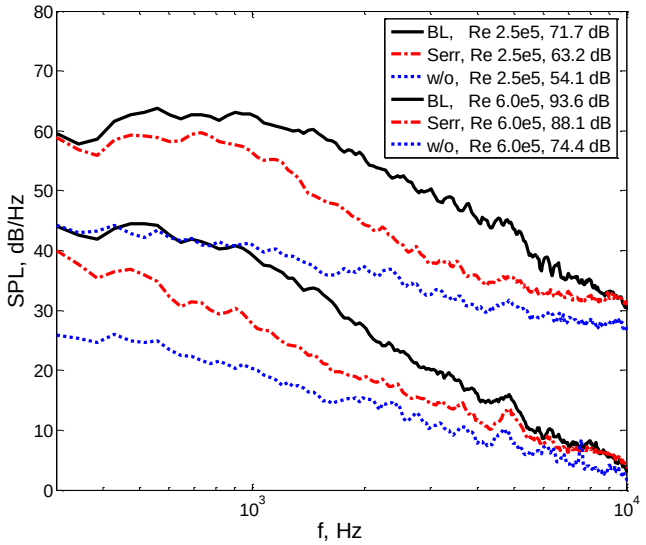

$$Tu(u) = \sqrt{u'^2} \Big/ \overline{U} \qquad (3)$$

Fig. 4 Comparison of the far field narrow band spectra at *Re* = 250,000 and 600,000 between the baseline *LE* (BL), serrated A45λ7.5 *LE* (Serr) and background (w/o) noises. Note that the background noise is without the airfoil but with the same turbulence grid and side-plates installed. Results at *Tu* = 5.5% and zero angles of attack. The *OASPL* is indicated in the box.

B. Amiet's Flat Plate Comparison

Figure 5 shows the non-dimensionalized far-field sound pressure level spectra for both the baseline and serrated cases. The *SPL* is scaled with the 4th power of the freestream velocity U_o, while the frequency is scaled with the airfoil semi-span and the U_o. The collapse of the spectra demonstrates that the *AGI*-noise can be accurately scaled with U_o^4 especially for the baseline *LE* case. A slight deviation can be observed for the serrated *LE* case, but generally the scaling law can still be applied in this case. This particular velocity dependency is consistent with the Amiet flat plate model [21].

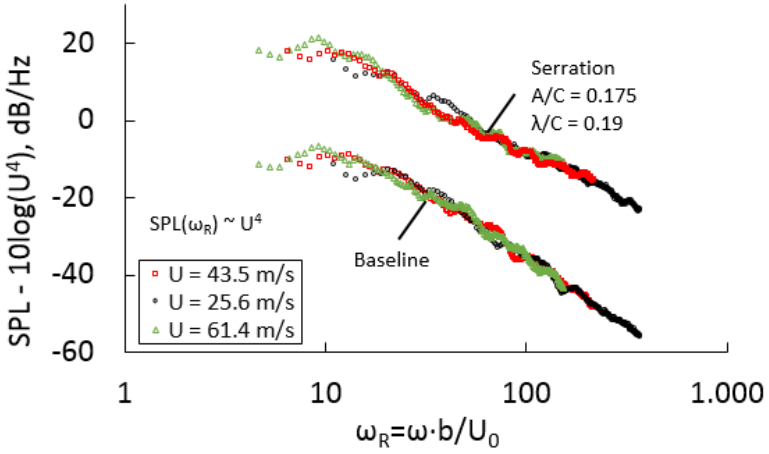

Fig. 5 Non-dimensionalized SPL spectra for the baseline and serrated *LE* at different flow velocities. The airfoil is set at *z/H* = 0 with *Tu* = 3.79 %. Note that the *SPL* for the serrated *LE* is shifted by 30 dB.

The Amiet model [21] was also used to validate the *AGI* noise produced by a baseline, straight *LE* airfoil in the current setting. The Amiet's model was modified slightly by taking into account of the consideration of the airfoil thickness according to Gershfeld [22]:

$$PSD(\omega) = \frac{2b}{\pi c}\left(\frac{2\Lambda_{uu}}{3\pi R}\right) Tu^2 \rho_0^2 U_0^4 \left[\frac{\Gamma\left(\frac{1}{3}\right)}{\Gamma\left(\frac{5}{6}\right)}\right]^2 \frac{\hat{K}_x^2}{\left(1+\hat{K}_x^2\right)^{\frac{7}{3}}}\, exp\left(\frac{-\omega \cdot d}{2U_0}\right) \tag{4}$$

$$where\ \hat{K}_x = -\frac{\omega}{U_0 k_e}\ and\ \ k_e = \frac{\sqrt{\pi}}{\Lambda_{uu}}\frac{\Gamma(5/6)}{\Gamma(1/3)}$$

where Λ_{uu} is the longitudinal integral length scale of the turbulence, *Tu* is the turbulence intensity, *R* is the observer distance, b the airfoil semi-span, d is the airfoil thickness and $\hat{K}_x$ is the normalized longitudinal wavenumber. The Λ_{uu} and *Tu* were measured independently. The model takes into account of the cross-power spectral density of the surface pressure on the airfoil caused by the turbulence.

Figure 6 shows the comparison of the power spectral density of the far field noise for the baseline, straight *LE* at three different flow velocities between the theory and experimental results. There is reasonably good agreement with Amiet's flat plate model for the mid-frequency range. The under-prediction at the high frequencies is mainly due to the dominance of the trailing edge self-noise. In case of the higher flow velocity, a larger discrepancy between the measurement and prediction is observed at the low frequencies. This can be attributed to the larger influence of the wind tunnel noise. At more extreme geometrical setting of the remaining parameters (e.g. increased angle of attack), however, the comparison between the measured noise and Amiet model becomes less accurate. This is mainly due to the increasingly mismatch between the Amiet's flat plate model and the NACA65(12)-10 airfoil with a significant *LE* curvature at large angle of attack.

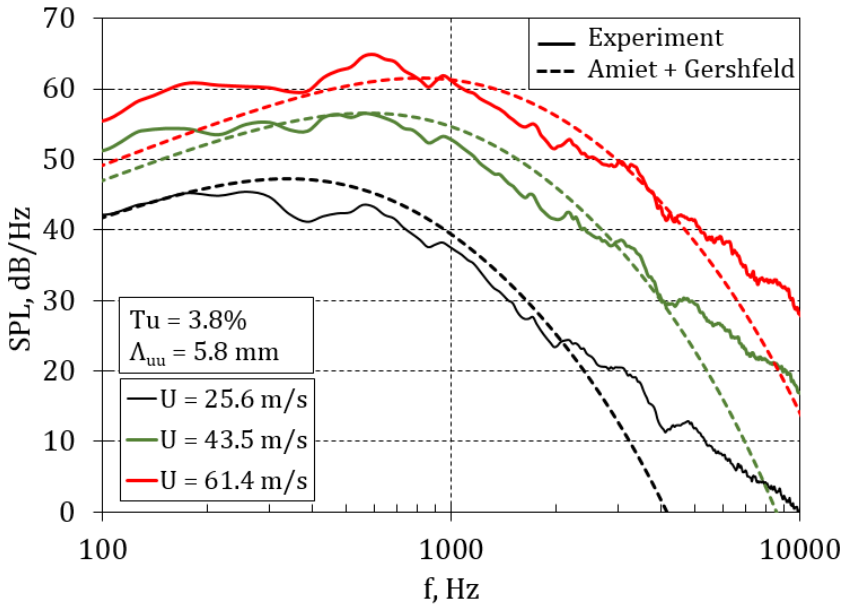

Fig. 6 Comparison between the Amiet's flat plate theory and the experiment results at Tu = 3.8 %, z/H = 0 and Λ_{uu} = 5.8 mm.

III. Statistical – Empirical Modelling Technique

Prior to the modelling, it is important to first identify meaningful target values for the present study. A set of five parameters, namely the Reynolds number (*Re*), the turbulence intensity (*Tu*), the serration amplitude (*A/C*), the serration wavelength (λ/C) and the angle of attack (*z/H*), were selected for the analysis. The main objective of the present work is to develop a statistical-empirical model to describe the independent effects and the interdependencies among the five influencing parameters on the *AGI* noise-reduction. For this purpose, the statistical Design of Experiments (DoE) approach was used.

When analyzing a defined physical experimental space by varying several influencing parameters, the classical method would be to vary one of the parameters, while the others remain constant. This procedure will then be repeated for each parameter of interest (raster method). This might be an easy and effective method to describe the influence of these parameters on a certain response variable with a high accuracy, as long as the number of parameters is small, and the interdependencies between the parameters are disregarded.

An increase of the parameters inevitably leads to an exponential rise of the necessary measurement trials (*MT*). According to the n-permutation in Eq. (5), analyzing a system with five parameters (*k*) and varying the parameters on five levels each (*n*) will result in 3125 trials. This represents a hardly manageable experimental volume. Instead, applying the statistical Design of Experiments (DoE) approach as per the Eq. 6 could lead to a significant reduction of the experimental volume to 43 trials without a significant loss of information on the system behavior. This approach keeps the experimental volume manageable and facilitates the detailed analysis of multiple parameters with a reasonably high accuracy.

$$MT_{n-per} = n^k = 3125 \tag{5}$$

$$MT_{DoE-CCD} = 2^k + 2 \cdot k + 1 = 43 \tag{6}$$

A. Design of Experiments (DoE) Methodology

The objective of the experimental modelling is the ability to describe the defined experimental space by means of functions that take into account of all the influencing parameters of significance (Eq. 7). For this purpose, the response variables (*RV*) have to be defined in order to act as target values of the regression functions. The coefficients are determined in accordance to the chosen set of influencing parameters (*IP*).

$$RV_i = f\left\{\sum_{j=1}^{n}\left(\left(IP_j + IP_j^2\right) + \sum_{k=1}^{n}(IP_j IP_{j+k})\right)\right\} \quad \begin{cases} i = 1..3 \\ j = 1..5 \\ k = 1..4 \end{cases} \tag{7}$$

The Design of Experiments methodology is based on the definition of an experimental space for a setup that consists a full factorial core [-1 ... +1], star points [-α ... +α] that label the upper and lower experimental boundaries, and a central point [0], which is defined as the experimental adjustment where all the parameters are on their intermediary values [23–26]. Based on this experimental composition of the DoE methodology, the analytical

statistic gathers the population from a subset. A circumscribed central composite design (*CCD*) was chosen as the appropriate experimental design. Circumscribed *CCD*s are characterized by statistical properties, such as the orthogonality or rotatability [27].

An experimental design is defined as rotatable, if the variance of the probability distribution is a function of the distance between the star point and the central point, and not of the direction, as is the case with orthogonality. Given a set of points within the experimental space at a constant distance to the central point, the rotatable design shows a consistent accuracy in the prediction for all the points. With regards to the statistical analysis, this property is highly advantageous [23]. On the contrary, the orthogonal designs are advantageous because they can avoid the confounding of the effects. This enables the determination of all the regression coefficients independently [28, 29]. In general, the α-values (star point locations) are higher than the coordinates of the central core ($\alpha_{DoE} > 1$), thus represent the limits of the experimental space. Consequently, each factor is varied as a combination of the five non-dimensional levels [+α, +1, 0, -1, -α]. A special design is the combination of both the properties in orthogonality and rotatability. As the requirements of orthogonality are not completely grantable while simultaneously guaranteeing the rotatability, this design is defined as pseudo-orthogonal and rotatable. It combines the advantages of both properties, especially because the resulting confounding is of negligible magnitude (< 0.02%).

As already described, the Design of Experiments approach is limited to describing the experimental space of interest by the functions of first and second order as well as linear interdependencies between the single influencing parameters (Eq. 7). In order to choose a valid model, preliminary investigations are necessary to ensure that the system satisfies these conditions. With this purpose all the five influencing parameters were analyzed individually in a preliminary study and their effects on the target values were evaluated carefully. This analysis, in combination with the defined experimental design, results in the test matrix as shown in Table 2, which also includes the upper and lower parameter settings. The total number of measurement point is 43, in addition to 16 repetitions for the central point in order to define a system-characteristic statistical spread, and to guarantee the desired statistical features. The trials of the strategically planned experiment were performed in a random order and they were repeated twice to obtain the average values. This procedure is to secure the reduction and elimination of unknown and uncontrollable quantities. Additionally, the analysis of the statistical significance allows the elimination of parameters with impacts on the response variable that is smaller than the statistical spread.

B. Response Variables

The response variables (*RV*) can be described by means of all influencing parameters in the first and second order as well as the interdependencies between the influencing parameters (Eq. 7). Defining the response variables is a crucial part of evaluating the experimental data. They are expected to describe the system with the necessary accuracy. This study focuses on the overall sound reduction of serrated *LE* compared to a baseline *LE*, and does not predict the *SPL* at a particular frequency. Consequently, the response variables of interest are limited to the *OASPL*. To define a sound pressure reduction level, information on both the baseline and the serrated *LE* are necessary. It is important to note that single microphone measurements were performed, hence, information on the sound directivity, overall sound power levels and sound power reduction are not available.

However, the dependencies of the sound generation itself are also of interest because it facilitates the analysis of the influence of each case on the reduction independently. As shown in Eq. (8), the noise produced by a baseline *LE* is a function of the Reynolds number, turbulence intensity and angle of attack. In the case of serrated *LE*, additional influences of the serration wavelength and amplitude must be taken into consideration (Eq. 9).

$$OASPL_{BL}[dB] = 20 \cdot log\left(\frac{\bar{p}_{BL}}{p_{ref}}\right) \rightarrow OASPL_{BL} = f\left(Re, Tu, \frac{z}{H}\right) \tag{8}$$

$$OASPL_{Serr}[dB] = 20 \cdot log\left(\frac{\bar{p}_{Serr}}{p_{ref}}\right) \rightarrow OASPL_{Serr} = f\left(Re, Tu, \frac{A}{C}, \frac{\lambda}{C}, \frac{z}{H}\right) \tag{9}$$

Note that p_{ref} = 2x10^{-5} Pa and the frequency range of interest is between 300 Hz and 10 kHz. Subtracting the $OASPL_{Serr}$ from the $OASPL_{BL}$ gives the overall sound pressure level reduction $\Delta OASPL$ (Eq. 10).

$$\Delta OASPL[dB] = OASPL_{BL} - OASPL_{Serr} = 20 \cdot log\left(\frac{\bar{p}_{BL}}{\bar{p}_{Serr}}\right) \tag{10}$$

IV. Selection of Key Noise Results

Generally, as shown in Fig. 7a, the serration amplitude is the main factor in reducing the broadband noise. At *Re* = 425,000, *Tu* = 3.79% and *z/H* = 0, the *LE* serration is found to be the most effective in frequency range between 850 Hz and 3500 Hz, where an average sound pressure level reduction of up to $\Delta SPL \approx 10$ dB is achieved by the largest serration amplitude (*A/C* = 0.3).

The turbulence intensity by itself was found to be another important factor that can dictate the level of broadband noise reduction. The narrow band spectra subjected to Tu = 2.08%, 3.79% and 5.5% under influencing parameters of Re = 425,000, z/H = 0, λ/C = 0.175 and A/C = 0.19 are plotted in Fig. 7b. It can be seen that the ΔSPL increases with increasing level of Tu. This effect is especially distinct in the intermediate frequency range of approximately 800 Hz to 4 kHz. It is important to note that the frequency range corresponding to the scenario when $\Delta SPL > 0$ broadens when the Tu increases. Increasing the Tu from low to intermediate values causes an increase of the upper frequency limit where noise reduction is still effective. A high Tu also leads to an increase of the noise reduction towards the low frequencies. More specifically, the level of broadband noise radiation for the baseline LE, and thus the $OASPL_{BL}$, increases with the level of Tu. Consequently, the noise reduction capabilities of the serrated LE are also the most effective at the elevated Tu condition.

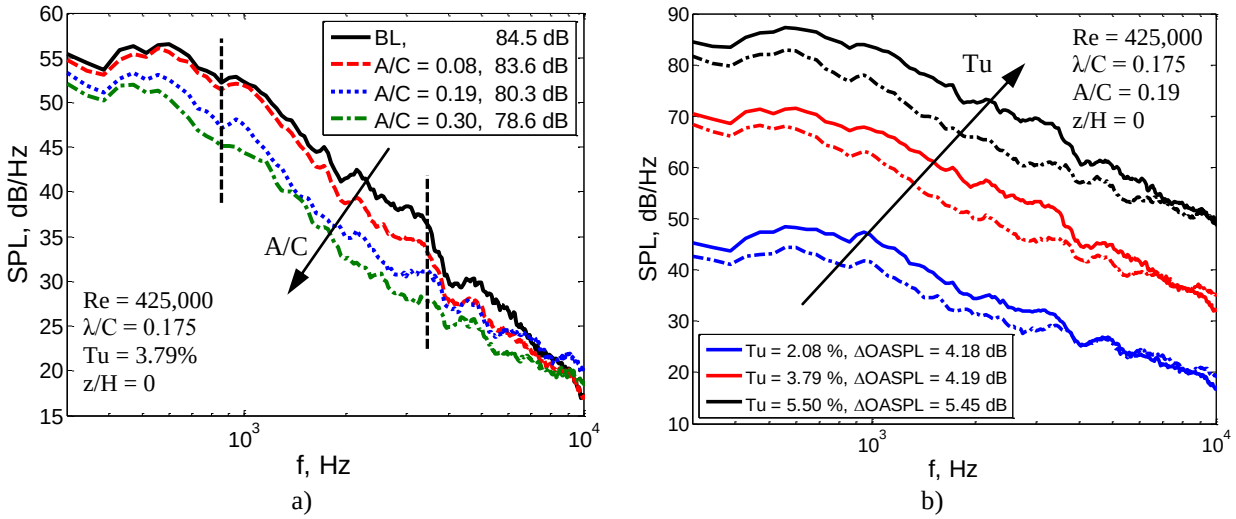

Fig. 7 The SPL spectra for the baseline (*BL*) and serrated airfoil at a) different serration amplitudes (*A/C*), where the vertical dashed lines indicate the frequency bandwidth of the noise reduction (850 Hz < *f* < 3.5 kHz), and b) different levels of *Tu*. The baseline *LE* and serrated *LE* are represented by the straight and dashed lines, respectively. Spectra correspond to the different *Tu* levels are shifted by 0 dB, 15 dB and 30 dB.

The noise reduction due to the serrated LE should increase linearly with frequency (at mid-to-high frequencies) until it is masked by the self-noise at high frequency, and little reduction should be expected at low frequencies. These characteristics can also be re-produced in the current experimental results. Figure 8 shows the ΔSPL spectra for a number of cases involving different serration wavelengths and amplitudes, as well as the turbulence intensities and Reynolds number. When the serration amplitude is fixed but with different serration wavelengths (Fig. 8a), the spectra demonstrate a linear increase of ΔSPL from mid-to-high frequencies until reaching ΔSPL ≈ 12dB for the one

with the smallest serration wavelength. After reaching this peak, the ΔSPL begins to drop at higher frequency due to the prominence of the self-noise radiation. As shown in Fig. 8b, when the serrated leading edge is subjected to different flow velocities, it produces the ΔSPL spectral shape that is very similar to those presented by Narayanan et al. [1] and Chaitanya et al. [3], i.e. the effective frequency range underpinning the ΔSPL will increase with increasing flow velocity. Figure 8c shows the influence of the serration amplitude on the ΔSPL spectra, which demonstrates that larger level of noise reductions can be achieved with a larger serration amplitude. This observation is consistent with the results reported by Narayanan et al. [1]. Finally, Fig.8d shows the influence of the freestream turbulence intensity on the noise reduction, which is consistent with the earlier results.

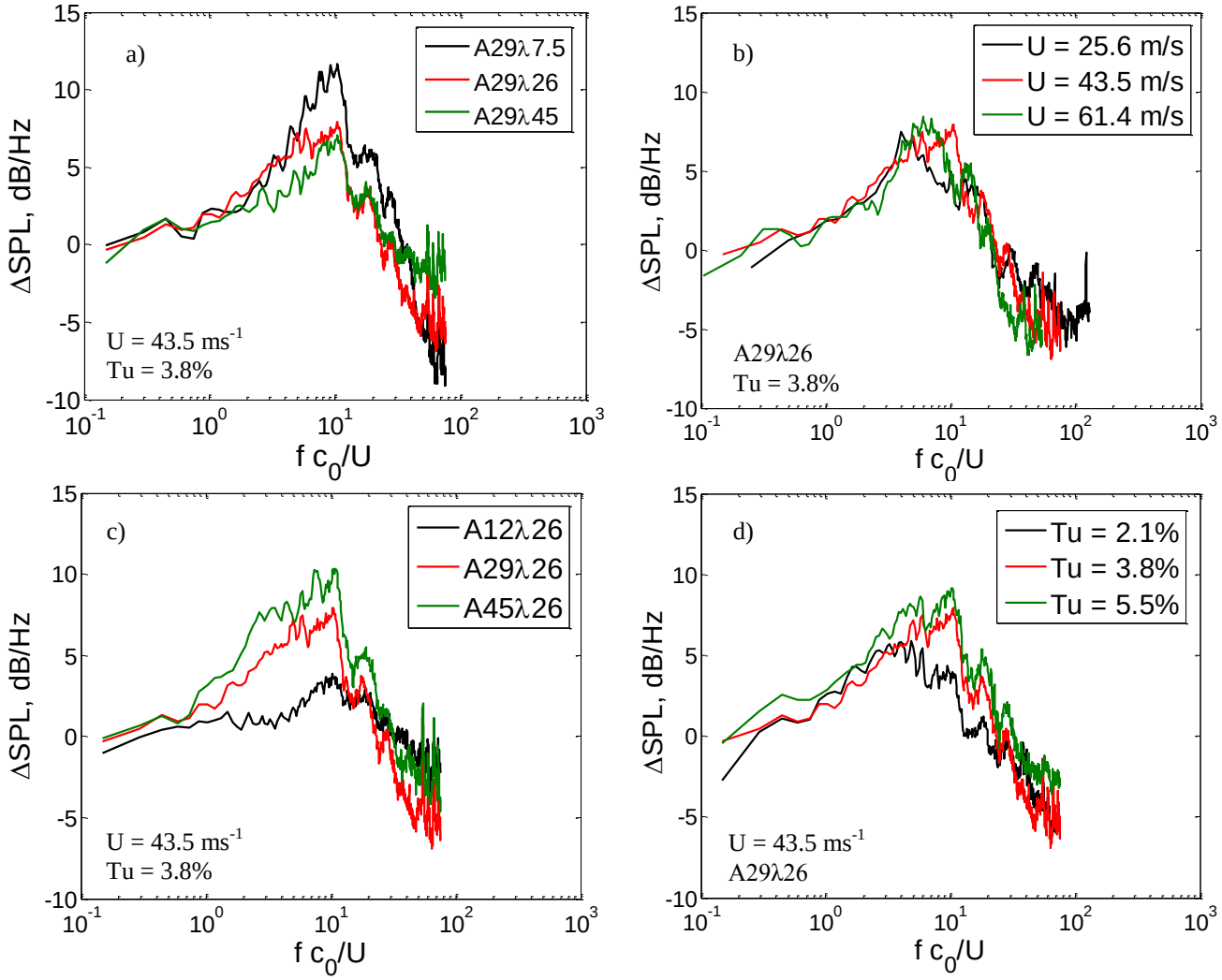

Fig. 8 The Δ*SPL* spectra at different a) serration wavelengths *λ*, b) Reynolds number *Re*, c) serration amplitude *A* and d) turbulence intensity *Tu*. Frequency normalized by Strouhal number Sr = f·C_0/U, where C_0 is the baseline chord length and U the free stream velocity.

A. General System Information

All four response variables were analyzed with the design of experiment methodology described earlier. Figure 9 shows the comparison of the experimentally-observed and the regression-predicted *OASPL* values produced by a serrated *LE*. The diagonal line represents a perfect match between the observed and predicted *OASPL*. Figure 9 shows that the measured *OASPL* for the serrated airfoil have an excellent agreement with the model, resulting in a standard deviation of 0.15 – 0.17%.

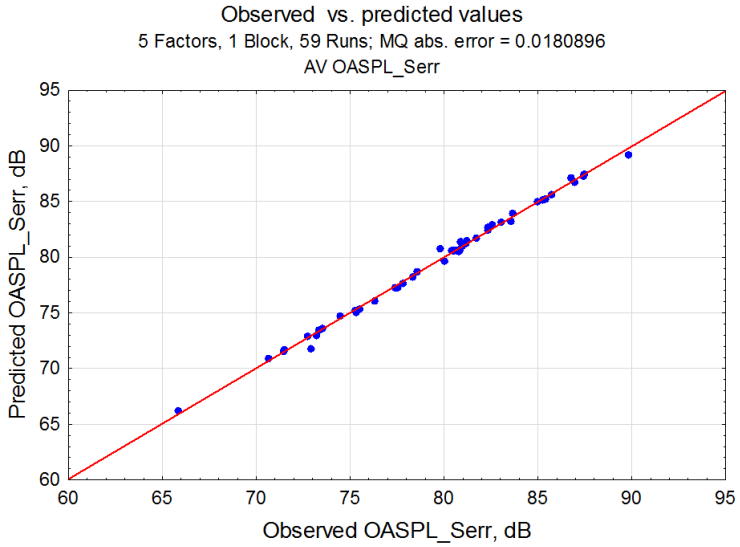

Fig. 9 Check of fit for the statistical-empirical model. Plot of observed vs. predicted values of the *OASPL* level produced by a serrated *LE*. There are 59 measurement points.

The radiated noise by a baseline *LE* was also analyzed at different Reynolds numbers, turbulence intensities and angles of attack. Note that the influence parameters of serration amplitude and serration wavelength are not included in the noise prediction for the baseline airfoil. The statistical spread rises slightly, however, when defining the Δ*OASPL* as uncertainties of the baseline and the serration prediction accumulate. For the first time, a ranking of the main factors and the interdependencies by means of their influence on the broadband noise reduction is presented. The Pareto diagrams in Fig. 10 show the enhancing (> 0) and suppressing (< 0) effects of the influence parameters on the target values. The Δ*OASPL* characterizes the sound reduction capability of the *LE* serrations. The diagram (Fig. 10b) shows that, in contrast to the response variables of the serrated noise in the absolute value of *OASPL* (Fig. 10a), the most dominant factor affecting the level of broadband noise reduction is the serration amplitude. The Reynolds number, previously the strongest enhancing factor for the absolute *OASPL*, seems to become less important for the sound reduction capability. Moreover, an increased influence of the serration wavelength on the

sound reduction is apparent in a linear and quadratic form. In general, the most significant dependencies of the overall sound pressure level reduction (Δ*OASPL*) demonstrated in this study are consistent with the findings of previous studies [3, 2, 30–33, 5, 34, 35].

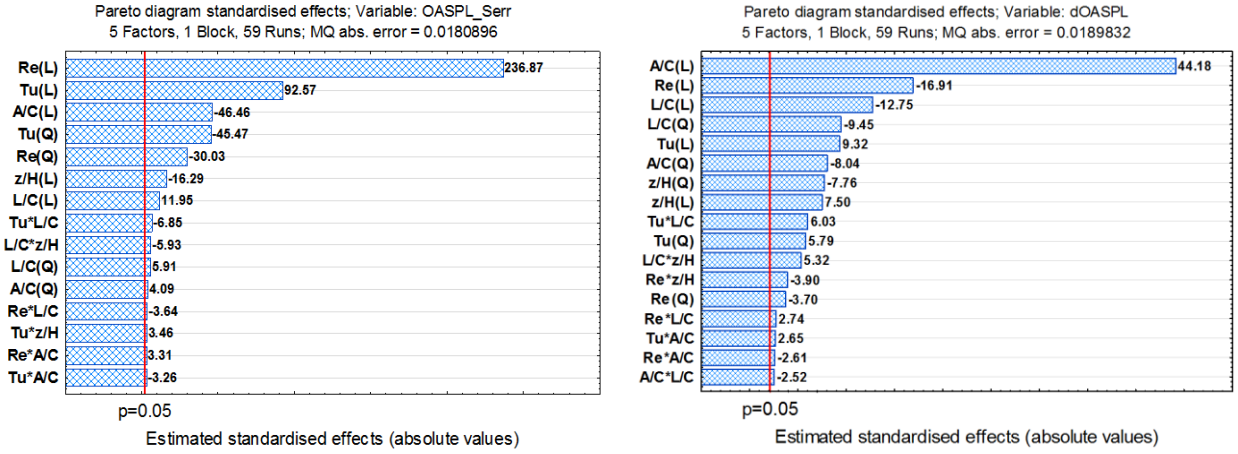

Fig. 10 Pareto diagrams. Ranking of enhancing (> 0) and suppressing (< 0) effects. The vertical line indicates the level of statistical significance (p = 5 %). Distinction between the linear (L) and quadratic (Q) effects are indicated. Response variable for a) *OASPL* by a serrated *LE*, and b) Δ*OASPL*.

The resulting sound pressure level for both the straight and serrated *LE*s, as well as the corresponding sound reduction, can be predicted with respect to the different influence parameters by the regression functions in Table 3. The model predicts the response variables by taking into account the statistically significant factors. Terms in red and *italic* represent factors whose influence is smaller than the statistical spread, and they can be added to the error term. This can reduce the complexity of the regression functions and keep the number of variables to a minimum.

Table 3 Functions of response variables defined as linear combination. Terms in red and *italic* indicate the influences which are smaller than the limit of the statistical significance (p = 5%).

Term	$OASPL_{BL}$ = [dB]	$OASPL_{Serr}$ = [dB]	Δ*OASPL* = [dB]
Constant	1.116E+01	6.780E+00	2.123E+00
Re (L)	+1.478E-04·*Re*	+1.437E-04·*Re*	+4.002E-06·*Re*
Re (Q)	-1.049E-10·Re^2	-9.310E-11·Re^2	-1.175E-11·Re^2
Tu (L)	+1.234E+01·*Tu*	+1.491E+01·*Tu*	-2.426E+00·*Tu*
Tu (Q)	-1.281E+00·Tu^2	-1.472E+00·Tu^2	+1.922E-01·Tu^2
A/C (L)	--	-3.800E+01·*A/C*	+4.994E+01·*A/C*
A/C (Q)	--	+3.249E+01·$(A/C)^2$	-6.538E+01·$(A/C)^2$
λ/C (L)	--	+1.352E+01· *λ/C*	-1.835E+00·*λ/C*
λ /C (Q)	--	+3.531E+01· $(\lambda/C)^2$	-5.787E+01·$(\lambda/C)^2$
z/H (L)	-1.142E+01·*z/H*	*-1.357E+01·z/H*	+4.658E+00·*z/H*
z/H (Q)	-5.152E+01·$(z/H)^2$	-5.638E+00·$(z/H)^2$	-4.574E+01·$(z/H)^2$
Re · Tu	*+6.323E-07·Re·Tu*	*+1.715E-07·Re·Tu*	*+4.608E-07·Re·Tu*
Re · A/C	--	*+2.327E-05·Re·A/C*	-1.876E-05·*Re·A/C*
Re · λ/C	--	*-2.221E-05·Re· λ /C*	+1.709E-05·*Re·λ/C*

Re* · *z/H	*-8.150E-06·Re·z/H*	*+1.574E-05·Re·z/H*	-2.389E-05·*Re·z/H*
Tu* · *A/C	--	*-2.349E+00·Tu·A/C*	+1.951E+00·*Tu·A/C*
Tu* · *λ/C	--	-4.268E+00·*Tu·* *λ/C*	+3.847E+00·*Tu·λ/C*
Tu* · *z/H	+3.069E+00·*Tu·z/H*	*+2.115E+00·Tu·z/H*	*+9.546E-01·Tu·z/H*
A/C* · *λ/C	--	*+2.290E+01·A/C·* *λ* */C*	-2.521E+01·*A/C·λ/C*
A/C* · *z/H	--	*+6.987E+00·A/C·z/H*	*-1.649E+01·A/C·z/H*
λ/C* · *z/H	--	-4.926E+01· *λ/C·z/H*	4.524E+01·*λ/C·z/H*

The intermediate effect on the influencing parameters within the experimental space on the overall noise reduction is plotted in Fig 11. The serration amplitude has the highest intermediate effect with an almost linear relationship between the *A*/*C* and Δ*OASPL*, before reaching an asymptotic level when the *A*/*C* is increased further. The serration wavelength *λ*/*C* shows a non-linear behavior where the optimum is achieved at intermediate wavelength, beyond which the noise reduction capability is weakened considerably. The predicted profile for the influence of the turbulence intensity *Tu* exhibits a large level of noise reduction at high *Tu* levels. On the contrary, at a band of low *Tu*, low level of noise reduction is predicted. This is in agreement with the measurements shown in Fig. 7b, where a high *Tu* is identified to be able to cause a high level of broadband noise radiation from a baseline airfoil. This in turn facilitates an increase of the noise reduction capability when a serrated *LE* is used. However, it is important to note that the effects of the individual parameters on the overall noise reduction in Fig. 11 cannot be attributed to the serrated *LE*s only. This is because different levels of *Re*, *Tu* and angle of attack (*z*/*H*) can also affect the baseline straight *LE*. Thus, a more detailed analysis of the noise reduction by the serration requires an independent analysis of the noise radiation by the baseline and serrated airfoil, respectively.

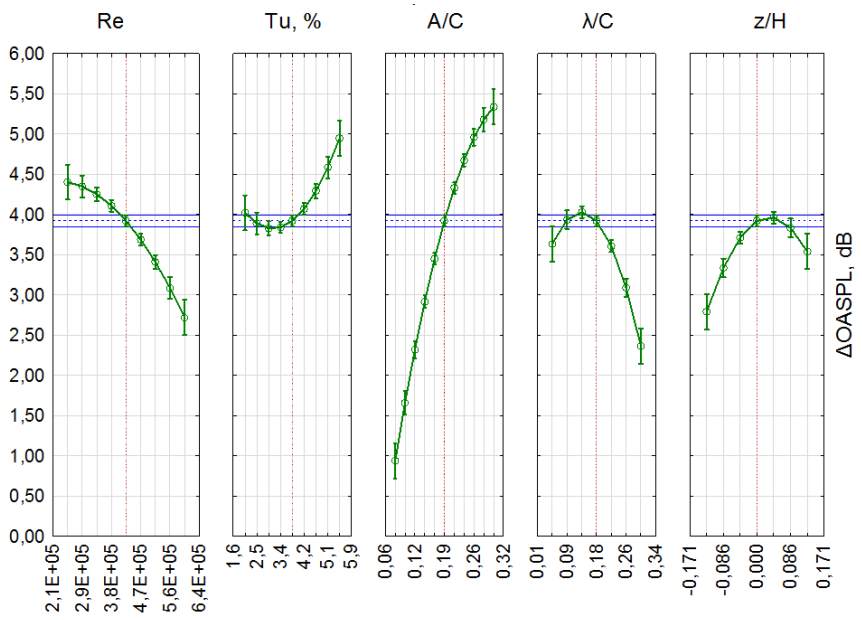

Fig. 11 Intermediate impact of the influencing parameters on the Δ*OASPL*, including the error band. The horizontal blue band indicates average noise reduction by the use of serrated *LEs*.

B. Interdependency of serration wavelength and turbulence intensity ($\lambda/C \cdot Tu$)

A significant effect identifiable in the response variable $\Delta OASPL$ was found to be an interdependency of the serration wavelength and the turbulence intensity ($\lambda/C \cdot Tu$), as can be seen in the Pareto diagram (Fig. 10b). At low *Tu*, small serration wavelengths are needed in order to achieve a high level of noise reduction, as exhibited by the red color region in Fig. 12. As the *Tu* is related to the integral length scale Λ_{uu} of the incoming gust, large serration wavelengths are expected to be less effective in the de-correlation effects especially if the incoming gust is characterized by small turbulent eddies. Previous investigations suggested that serration wavelengths should be small to achieve good level of noise reduction, although in general the impact of the serration wavelength is not as dominant as the serration amplitude [3, 5, 2]. The interdependency in Fig. 12 shows that the optimum serration wavelength highly depends on the incoming *Tu* level. Low to intermediate *Tu* support the previous findings that a smaller serration wavelength is more desirable. However, at high *Tu*, serration wavelengths of intermediate values are far more effective in reducing the *OASPL*, as shown in Fig 12. This agrees with the finding of a recent work [3], where the optimum serration wavelength is found to be twice the size of the incoming turbulent structure in the form of the integral length scale Λ_{uu}. An optimal set of *Tu* and λ/C leads to a reduction of the fluctuating acoustic pressure of about 53% to that produced by the baseline airfoil.

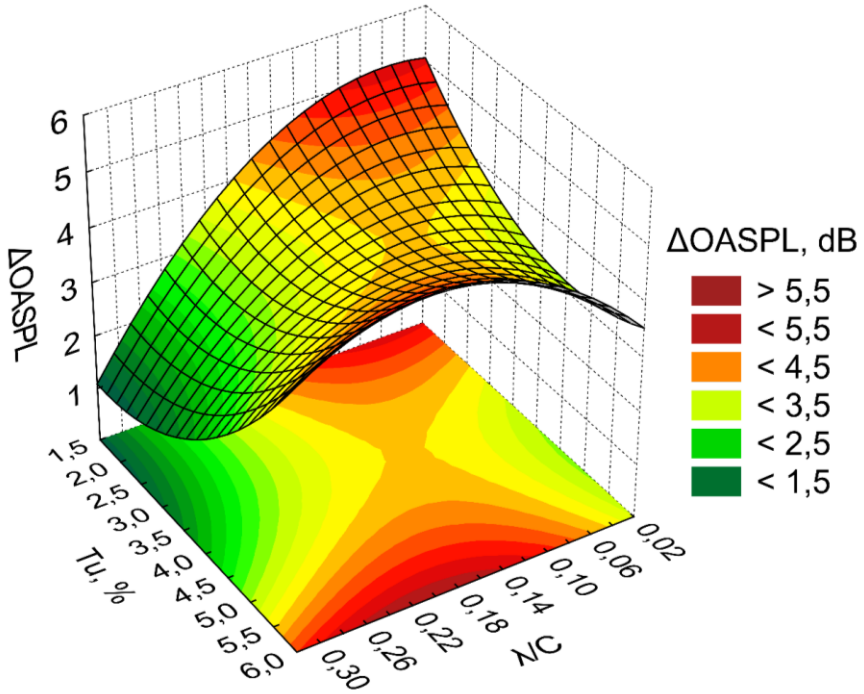

Fig. 12 Influence of interdependency between the serration wavelength (λ/C) and turbulence intensity (*Tu*) on the $\Delta OASPL$. Other influencing factors remain on intermediate levels (*Re* = 425,000, *A/C* = 0.19, *z/H* = 0).

In order to gain a deeper insight in the underlying principles, the acoustic spectra at Re = 400,000, A/C = 0.2 and z/H = 0 have been analyzed in more detail. Figure 13 shows the influence of the serration wavelength at Tu = 5.5% (Fig. 13a) and at Tu = 3.2% (Fig. 13b) and compares them to the baseline case. In general, high turbulent inflow causes an *OASPL* which is about 4.5 dB higher compared to the low turbulent case for the baseline airfoil. The serrated *LE*s respond more sensitively at high Tu for the *OASPL* regardless the level of the serration wavelength, where up to 4.8 dB in $\Delta OASPL$ could be achieved. For the low Tu case, however, there is a wider spread of the noise reduction efficiency among the different serration wavelengths, where a low serration wavelength tends to achieve higher noise reduction especially in the low frequency region of 300 Hz $\leq f \leq$ 2 kHz. This supports the interdependency described previously as the level of noise reduction differs only slightly when varying the serration wavelength at high Tu; at low or intermediate Tu, large serration wavelengths become ineffective in the noise reduction. Moreover, in the low frequency region the noise reduction for the intermediate to large serration wavelengths mainly takes place at frequencies $f \leq$ 4 kHz. However, in the high Tu case the noise reduction occurs up to f = 6 kHz albeit the comparatively low energy level in the high frequency region prevents significant changes in the overall sound pressure level.

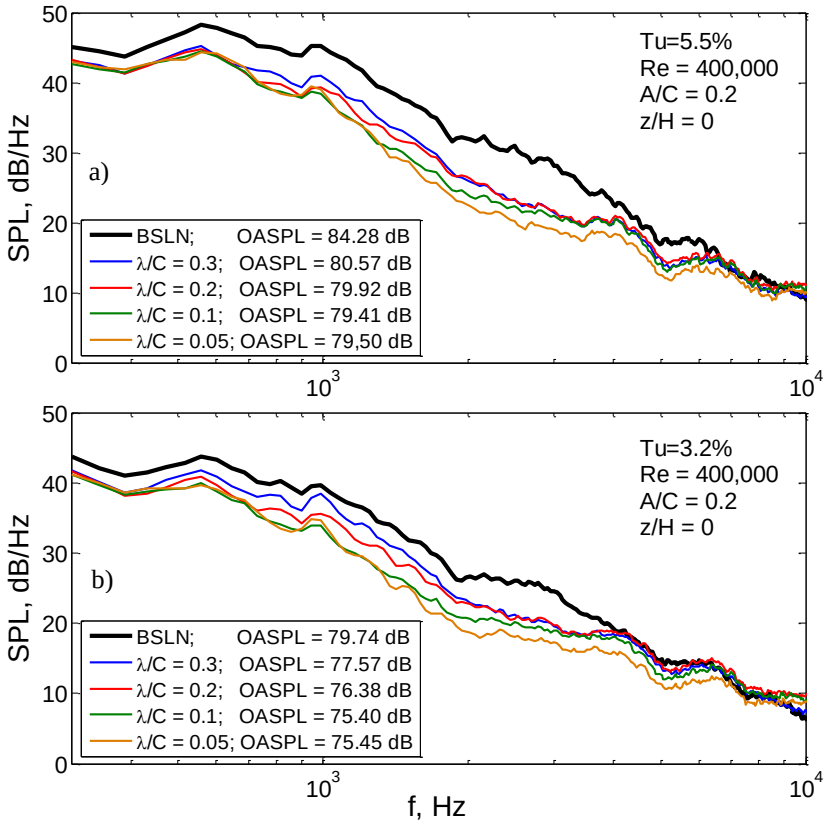

Fig. 13 Narrow band spectra for the different serrations wavelength at a) *Tu* = 5. 5% and b) *Tu* = 3.2%. The remaining parameters remain on constant, intermediate levels at *Re* = 400.000, *z/H* = 0, *A/C* = 0.2.

C. Interdependency of angle of attack and serration wavelength (*z/H* ·*λ/C*)

In addition to the interdependency between the turbulence intensity and serration wavelength described previously, another interdependency between the angle of attack and the serration wavelength (*z/H* ·*λ/C*) was also found to be significant, as shown in Fig. 14. In general, the level of noise reduction by the serrated *LE*s is the maximum at zero angle of attack, which is in agreement with other authors [2, 3]. However, at a large negative *z/H* (or *AoA*), small serration wavelengths are needed to achieve a reasonably large noise reduction (red color region), whereas serration wavelengths of intermediate dimensions are preferable at large positive *z/H*. The underlying principle of this interdependency could be related to the specific semi-cyclic shape of the *LE* serrations relative to the stagnation point of the incoming flow. In the case of zero angle of attack, the serration wavelength that can achieve the largest noise reduction is defined by how well it can de-correlate the spanwise coherence of the turbulence eddies, and how efficient it can facilitate a "nozzle" effect to accelerate the flow from the serration tip to the serration root and reduce the *Tu* level. At a negative *z/H*, the projected area of the upper surface of the *LE* will

cause a significant impingement upon the incoming gusts. In this case, the use of small wavelength serrations is a logical choice.

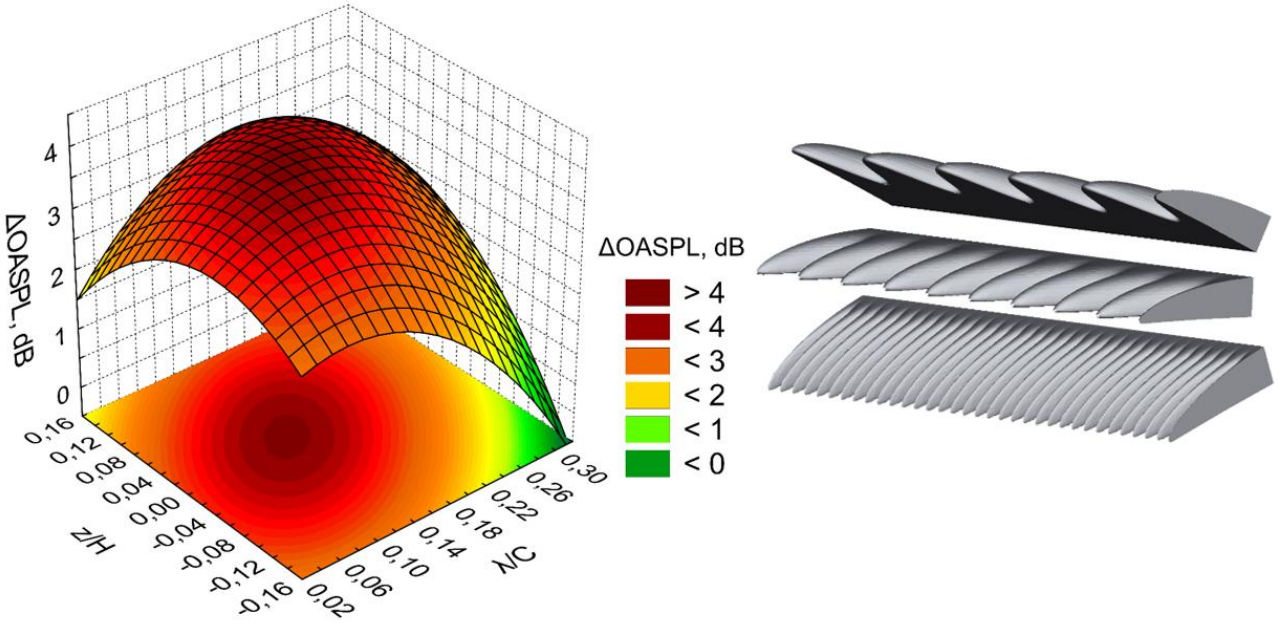

Fig. 14 Influence of interdependency between the serration wavelength and angle of attack ($\lambda/C \cdot z/H$) on the Δ*OASPL*. Other influencing factors remain on the intermediate levels (*Re* = 425,000, *A/C* = 0.19, *Tu* = 3.8%).

This is because a small serration wavelength will cause many three-dimensional undulations on the upper surface of the *LE*, which will maintain the serration effect to achieve the interaction noise reduction.

In the case of a positive *z/H*, the incoming flow will naturally impinge on the lower surface of the *LE*. However, the planar geometry at the lower surface of the serrated *LE* means that the three-dimensional undulation can no longer be achieved by using a small serration wavelength. Instead, a larger serration wavelength is preferable to avoid the direct impingement between the incoming gusts and the *LE* geometry.

Of particular interest is the impact of this interdependency ($z/H \cdot \lambda/C$) on the narrow band spectral characteristic. It has already been known that the smallest serration wavelength does not necessarily lead to a maximum noise reduction across the whole frequency range [2]. A first indicator for the effect of small serration wavelengths on the noise can be found in the high frequency region above 10 kHz (Fig. 15), where all the different serration wavelengths actually lead to noise increase. It is clear that the largest noise increase occurs at the smallest serration wavelengths. However, this effect is neglected in the present study because the lower and upper frequency limits for

the *OASPL* analysis are taken at 300 Hz and 10 kHz, respectively. Within this frequency range, the noise reduction capability usually improves when the serration wavelength reduces.

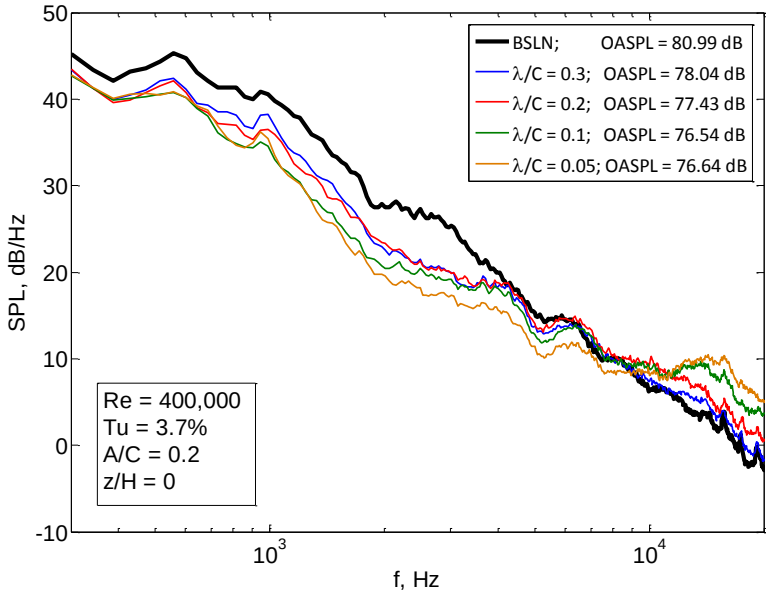

Fig. 15 Narrow band spectra produced by the baseline and serrated *LE*s of different serration wavelength at *Re* = 400,000, *Tu* = 3.7%, *A/C* = 0.2 and *z/H* = 0.

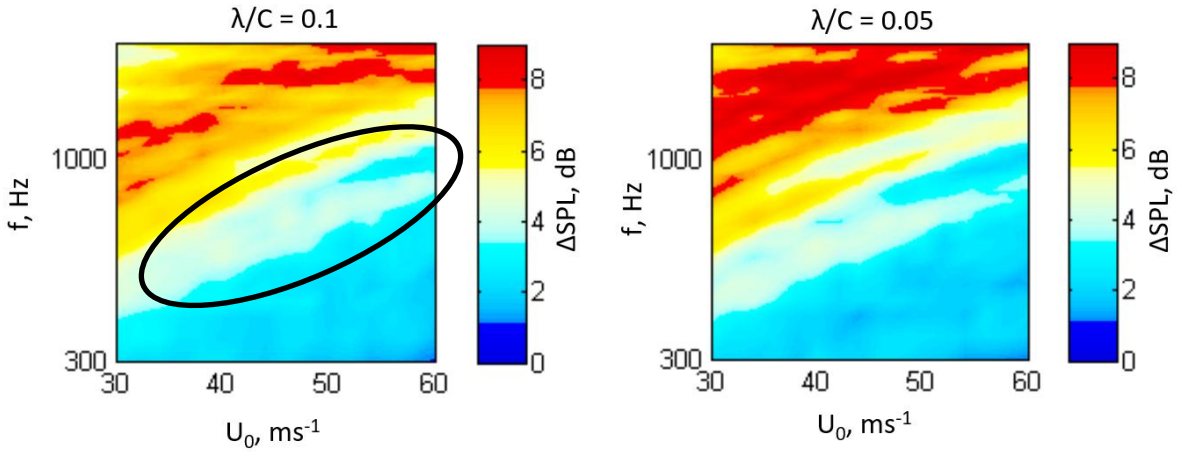

a) b)

Fig. 16 Contours of Δ*SPL* as a function of *f* and *Uo*. The serrated *LE*s have the common influence parameters of *A/C* = 0.2, *z/H* = 0 and *Tu* = 3.7%, but at different a) λ/C = 0.1 and b) λ/C = 0.05.

The impact of the serration wavelength on the low frequency region can be examined in Fig. 16 where the noise reduction Δ*SPL* of a serrated *LE* with the intermediate (*λ/C* = 0.1) and a small serration wavelength (*λ/C* = 0.05) are compared with each other as a function of the inflow velocity and frequency. Above *f* = 1 kHz the noise reduction is

significantly higher for the small serration wavelength (Fig. 16b). However, as indicated by the circled black region in Fig. 16a, the level of noise reduction is higher for the intermediate wavelength in a frequency range of 500 Hz ≤ f ≤ 1.2 kHz. As a result, the $\Delta OASPL$ is slightly higher for the intermediate λ/C = 0.1 case.

Figure 17 shows the *SPL* spectra produced by the baseline and serrated *LE*s of a slightly larger serration wavelength (λ/C = 0.175) at different angles of attack *AoA* (or z/H). At first glance, it is clear that the largest level of noise reduction occurs at $z/H > 0$ and across the widest frequency range (Fig. 17a). The level and frequency range of the noise reduction are lessened as the z/H decreases. However, a closer examination shows that the sensitivities of the *SPL* and *OASPL* to the z/H are different between the baseline and serrated *LE*s. For the baseline *LE*, the lowest *OASPL* is achieved at $z/H < 0$ what is mainly due to the low level of noise radiation in the frequency range of 2 kHz ≤ f ≤ 4 kHz. The largest level of *OASPL* produced by the baseline airfoil, on the other hand, is achieved at $z/H = 0$. The noise level produced at $z/H > 0$ lies in between. For the serrated *LE*, the lowest level of the *OASPL* is achieved at $z/H > 0$. As the z/H slowly decreases, the level of *OASPL* increases. This contradictory behavior between the baseline and serrated *LE*s for the noise radiation should be taken into consideration when examining the interdependency ($z/H \cdot \lambda/C$) for the ΔSPL or $\Delta OASPL$.

In Fig. 17c, when the airfoil is set at $z/H = -0.128$, there is little noise reduction at 1.2 kHz ≤ f ≤ 3.8 kHz because of the opposite trends in *SPL* produced by the baseline airfoil (reduction in the *SPL* level) and serrated airfoil (increase in the *SPL* level), respectively. At f > 3.8 kHz, the serrated *LE* even causes a significant noise increase which is not due to the experimental error as we have re-tested it many times. Rather, the presence of the serration wavelength actually facilitates cross-flow from the projected upper surface of the *LE*, through the serration air gaps and exits the lower surface of the *LE*. This particular fluid–structure interaction causes the noise to increase at high frequency that will otherwise be absence in a baseline *LE*. This conjecture is supported by the clear trend from other results where the noise increase at high frequency will gradually cease to exist when the angle of attack increases.

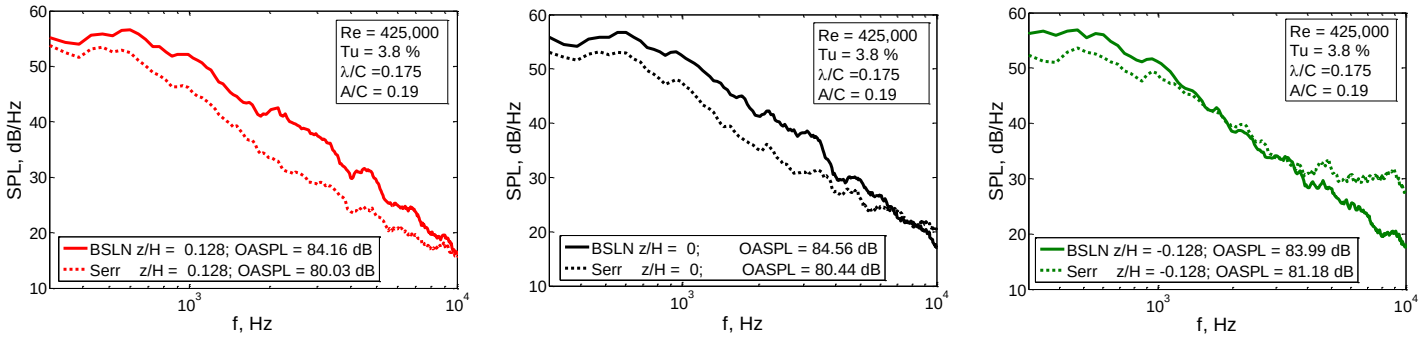

Fig. 17 Narrow band spectra (300 Hz < *f* < 10 kHz) for the noise produced by the baseline *LE* (solid lines) and serrated *LE* (dotted lines) at a) *z*/*H* = 0.128, b) *z*/*H* = 0 and c) *z*/*H* = -0.128

D. Model Refinement

Complementary measurements were carried out in the outer regions of the defined experimental space to test the stability of the statistical model, especially at the extreme settings of the influencing parameters. The measurement results were found to fit well to the model, although an increase of prediction uncertainty was observed with multiple factors on the extreme levels, which statistically represents a large distance between the central point and the measurement locations. In general, the model was found to predict the absolute level of noise radiation (*SPL* and *OASPL*), and the level of noise reduction (ΔSPL and $\Delta OASPL$) reasonably accurate.

However, up to now, the model is based on a data set of 59 measurement trials, including the measurement of the central point for 17 times in a randomized order to describe the statistical spread of the model. In order to improve the stability of the developed model, additional data points were incorporated from an independent previous study, which took place under the same measurement conditions, but with different leading edge serrations and flow parameters [2]. The measurement results from the previous study are combined with the current model to increase the total measurement points to 285. This improved model serves as a data base to predict the noise radiation by the serrated *LE* at various configurations, as well as the noise reduction when compared with the baseline airfoil. The additional measurement results are based on eight serration designs (see the table within the Fig. 18a), which were tested in a velocity range of 20 $ms^{-1} \leq U_0 \leq 60$ ms^{-1}, or Reynolds number of $200{,}000 \leq Re \leq 600{,}000$, respectively. The turbulence level was varied by interchanging three grids that yield *Tu* = 3.2 %, 3.7 % and 5.5 %. The angle of attack was altered from $-0.102 \leq z/H \leq 0.128$, or -8 deg ≤ *AoA* ≤ +10 deg, respectively. The extended model was found to fit well to the initially developed algorithm as indicated by the regression curve for the *OASPL* in Fig. 18b.

The fit of regression shows a good match of high order when comparing between the observed and predicted values for the *OASPL* by the serrated *LE*.

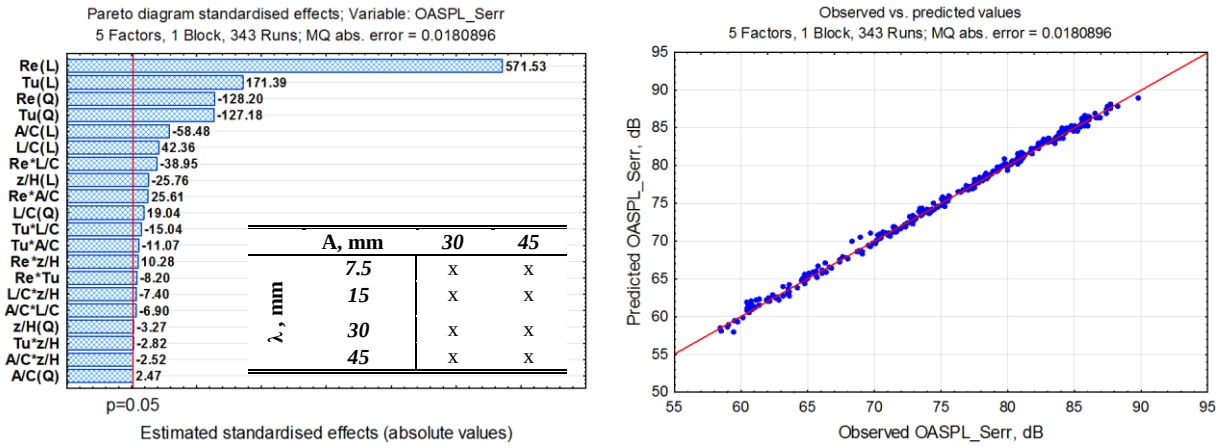

a) b)

Fig. 18 Check of model validity for the serrated *LE* noise ($OASPL_{Serr}$). a) Pareto diagram for the extended model. The insert table shows the test matrix for additionally serration parameters at $200{,}000 \leq Re \leq 600{,}000$ and $-0.102 \leq z/H \leq 0.128$ from [2] and b) Plot of observed vs. predicted values of the $OASPL_{Serr}$ comprising 285 measurement points (initial reference model is shown in Fig. 9).

If the original model (Fig. 10a) is compared with the refined one (Fig. 18a), the dependencies are found to be the same order and magnitude for the *OASPL* and Δ*OASPL*. When examine the Fig. 18a, the modified interdependency plot between the *Re* and λ/C for the *OASPL* of serrated airfoil remains almost unaffected by the additional data points, although it is expected to be more reliable due to the increased data pool. This is manifested in Fig. 19 where the blue circles indicate the underlying set of data on which the model was established. Despite a significant increase of the amount of experimental data in Fig. 19b, the shape and magnitude of the interdependency remain almost constant.

To conclude, the additional data pool in the modified model has a negligible impact on the main factors and the reliability of the original model which uses less data points. Furthermore, all the interdependencies remain very similar although there are slight changes in the magnitude as a result of the additional data pool. Therefore, the results presented in this section confirm that the original statistical-empirical model is still stable and reliable.

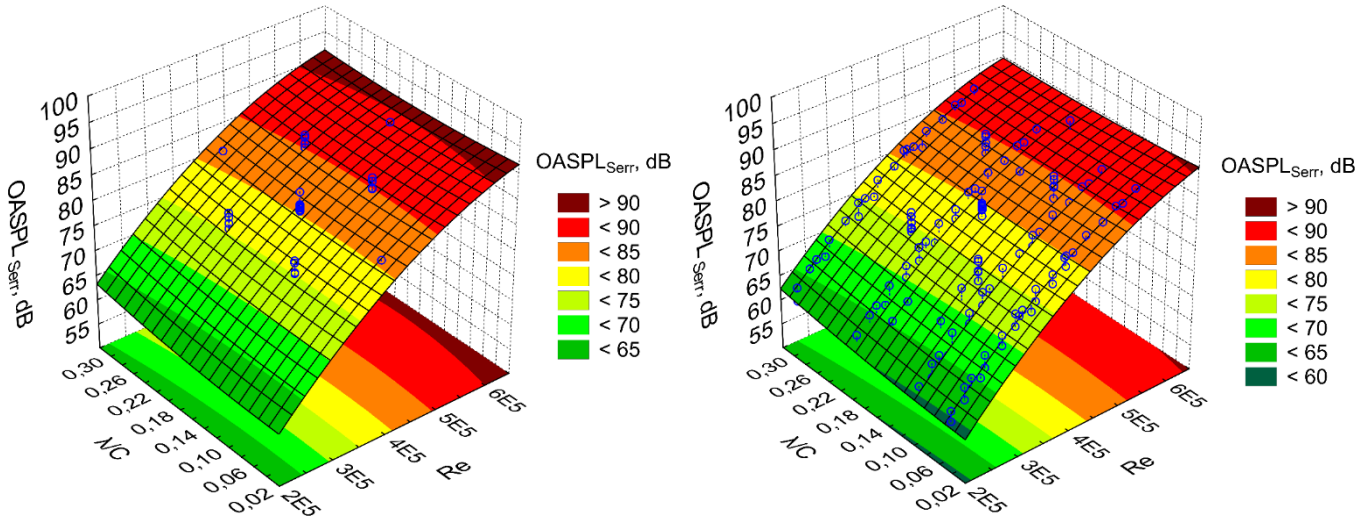

a) b)

Fig. 19 Comparison of interdependency between the ($Re \cdot \lambda/C$) for the a) original model, and b) improved model by the use of additional data points (circles) obtained from [2].

E. Polyoptimum of noise reduction and noise radiation

The purpose of the current system is to reduce the broadband *LE* noise caused by the interaction between the high turbulent inflow conditions and the *LE*. Therefore, in addition to the main focus on achieving high level of noise reduction as defined by the relative difference between airfoils with straight and serrated *LE*s, it is also desirable to produce low absolute magnitude of the overall sound pressure. An algorithm has been developed to define a polyoptimum of the radiated noise and the noise reduction capability by the serrated *LE*s.

Of further interest is the qualitative information on the impact of the different influencing parameters on the polyoptimum. As shown in Fig. 20 the independent response variables $OASPL_{Serr}$ and $\Delta OASPL$ were weighted with an emphasis on the reduction of the *OASPL*. This means that the *OASPL* is weighted linearly between 50 – 70 dB where 50 dB equals to an acceptability of 100%. In contrast, the $\Delta OASPL$ accounts for zero percent acceptability at 2 dB with a slope of 2 until reaching the desired optimum of 10 dB overall noise reduction (100% acceptability).

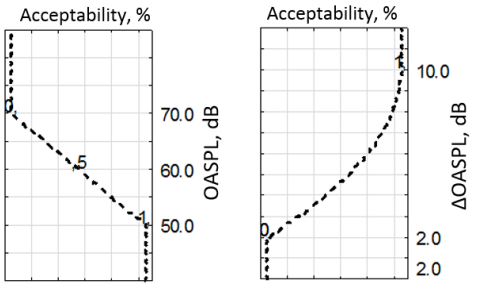

Fig. 20 Weighted functions of the single analyzed response variables.

Figure 21 shows the polyoptimum of noise radiation and noise reduction with serrated *LE*s. The first row shows the dependencies on the noise radiation (*OASPL*) where the *Re* effect is clearly the most influential. It is then followed by the *Tu* and *A*/*C*. The λ/C and *z*/*H*, on the other hand, can be considered as the secondary importance. The effects of the influencing parameters on the noise reduction ($\Delta OASPL$) are shown in the second row of Fig. 21. With the exception of the *Tu*, the rest of the influencing parameters exert reverse trend between the *OASPL* (for the serrated *LE*s) and the $\Delta OASPL$. For example, an increase of the *Re* would increase the *OASPL*. As a result, the $\Delta OASPL$ will reduce. A maximum noise reduction of $\Delta OASPL$ = 7.5 dB, while maintaining a relatively low noise radiation of *OASPL* = 53.8 dB, is reached at the minimum *Re*, *Tu* and λ/C in combination with the maximum *A*/*C* and *z*/*H*. As shown in the third row in Fig. 21, the contribution of each of the parameters to the polyoptimum, which is defined as the acceptability, spreads over large margins. In order to achieve a minimum absolute level of noise radiation while maintaining a high noise reduction capability of the serrations, one could utilize the algorithm of the polyoptimum to optimize the effective degrees of freedom when other design parameters are fixed.

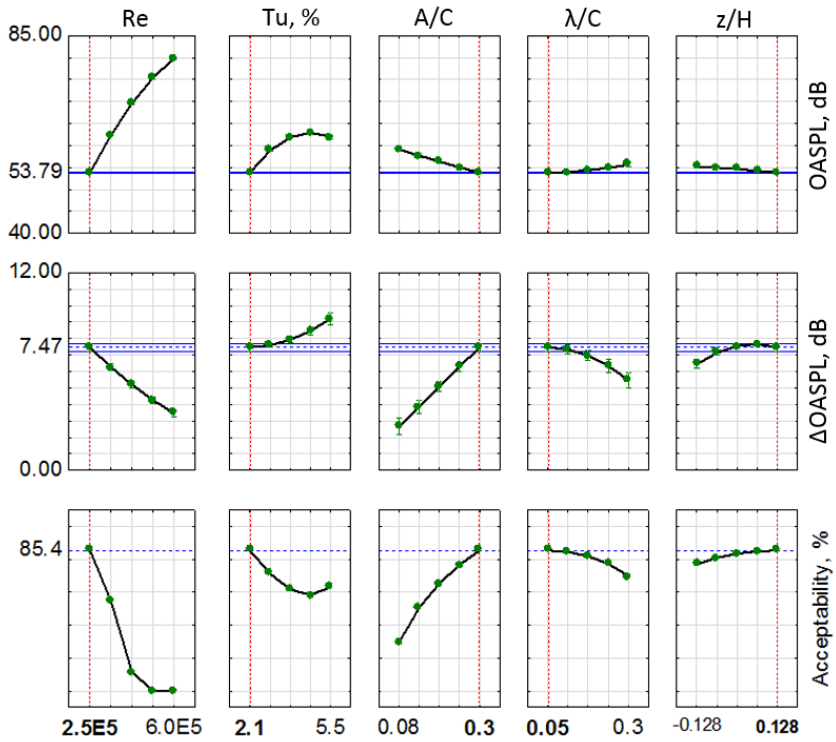

Fig. 21 Polyoptimum of the *OASPL* (top row) and the noise reduction capability Δ*OASPL* (center row), as defined by the function of acceptability (bottom row and Fig. 20)

F. Model Validation with External Data

To validate the statistical-empirical model developed in this paper, the predicted *OASPL* and Δ*OASPL* are compared with external data obtained independently in the DARP Aeroacoustic Wind Tunnel at the Institute of Sound and Vibration Research (*ISVR*), University of Southampton [3]. The model was scaled in accordance with the different experimental conditions (e.g. microphone measurement locations) before the comparison was made. The airfoil used in *ISVR* is the same type (NACA 65(12)-10) with a chord length C = 150 mm and a span of S = 450 mm. The authors forced a bypass transition of the boundary layer from laminar to turbulent by the tripping tapes in order prevent the production of the laminar instability tonal noise [3]. At elevated level of freestream turbulence the *LE* noise is considered to be the dominant noise source. Therefore in this case the boundary layer tripping can be assumed to have no influence on the radiated noise [36, 37]. The tests in *ISVR* were performed by the use of serrated sinusoidal *LE*s, defined by the amplitude, with a peak-to-trough ratio of 2h and the wavelength λ. Note that there is a difference in the definition of the serration parameters, where *ISVR* adopted the "*same wetted-area*" principle. This means that for the same serration amplitude, $A = 2h$, the serration peak would extend the initial airfoil chord length

by h, giving an overall chord of ($C + h$). Accordingly, the serration root would, retracted by h, give an overall chord of ($C - h$).

The turbulence intensities at the *ISVR* were generated at Tu = 2.5% and 3.2%, and the incoming flow velocities are U_0 = 20 ms^{-1}, 40 ms^{-1}, and 60 ms^{-1}. The difference in distance of the far field microphone location is corrected by use of the monopole scaling law according to Eq. (11).

$$SPL(R_2) = SPL(R_1) - \left|20 \cdot log\left(\frac{R_1}{R_2}\right)\right| \rightarrow \Delta SPL = \left|20 \cdot log\left(\frac{R_1}{R_2}\right)\right| \tag{11}$$

where R_1 and R_2 are the absolute distances between the source and the observer (measurement location) at a polar angle of Θ = 90 deg. Differences in the span were also compensated by a linear scaling. Twelve measurement points were analyzed at zero angles of attack and Tu = 2.5%. The Reynolds numbers were matched at Re = 394,000 and 624,000. The serration amplitudes are varied by 0.1 < A/C < 0.35, and the serration wavelengths are varied by 0.05 < λ/C < 0.25.

Applying the specific boundary conditions of the *ISVR* test rig to the current model yields the predictions of the *OASPL* for both the baseline and serrated airfoils, which are shown in Fig. 22. It is clear that excellent agreement has been achieved between the predicted and measured data. The overall noise reduction Δ*OASPL* also demonstrates a good agreement with the predictions, although with a slightly larger discrepancy due to the accumulated errors in the *OASPL* radiated by both the baseline and serrated airfoils.

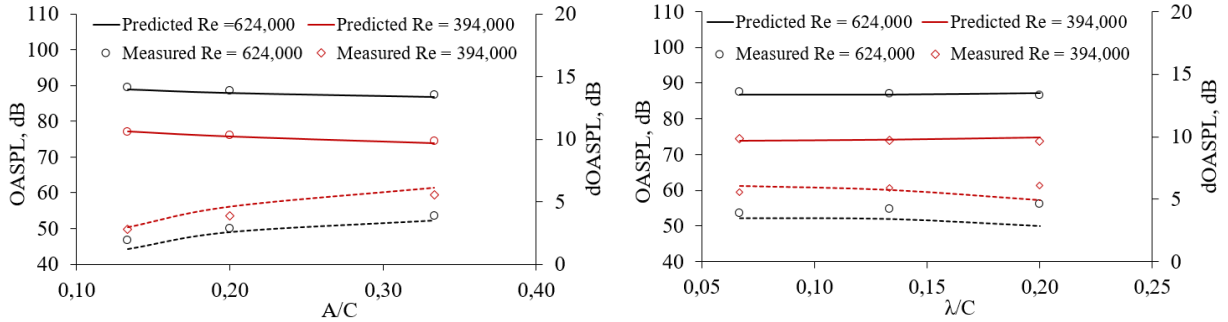

Fig. 22 Validation of the current statistical-empirical model with external experimental data provided by *ISVR, University of Southampton* [3] at different a) serration amplitudes, and b) serration wavelengths. Predicted *OASPL* with serrated *LE* (solid lines) and Δ*OASPL* (dotted lines). The circle and diamond symbols represent the experimental results by the *ISVR*.

The *OASPL* reduces when the serration amplitude increases, as predicted by the model. The influence of the serration wavelength shows a different behavior. The predicted data underlines a decreasing Δ*OASPL* with

increasing serration wavelength (Fig. 22b). This trend contradicts with the *ISVR*'s experimental findings, which show that the $\Delta OASPL$ increases slightly with the serration wavelength. The discrepancies between the predicted and measured values are up to 1.2 dB at the largest serration wavelength. Altogether, the current statistical model can still be regarded as a robust tool for the predictions of the *AGI*-broadband noise subjected to serrated *LEs*.

V. Conclusion

An experimental aeroacoustic study was performed to quantify the effects of five influencing parameters on the Airfoil-Gust-Interaction broadband noise of a NACA65(12)-10 airfoil and the noise reduction achieved by the serrated leading edges. For the statistical-empirical modelling, the Design of Experiments (DoE) technique was utilized to reduce the experimental volume to a manageable amount in order to gain information on the interdependencies of each influencing parameter and to develop a prediction tool that describes the overall noise radiation. The model, initially based on 59 measurement points, was validated to be accurate. It is then further stabilized by extensive additional data set. It shows an accurate performance at settings close to the defined central point of the experimental space, and is only slightly less accurate in the outer regions of the pre-defined setting ranges. When the predicted results are compared with the external data which was acquired in a separate experimental setting, the excellent agreement indicates that a robust and reliable statistical-empirical model has been developed in this study. The aeroacoustic results allow the current paper to reach the following conclusions:

- A clear ranking and quantification of the influencing parameters, where the Reynolds number (*Re*) and the freestream flow turbulence intensity (*Tu*) are the main contributors to the broadband noise emissions. On the other hand, the serration amplitude (*A/C*), followed by the *Re* and the serration wavelength (λ/C) would represent the main factors for an effective broadband noise reduction.
- Identification of a significant interdependence of the serration wavelength and the freestream turbulence intensity ($\lambda/C \cdot Tu$) with regard to the overall noise reduction capability. This feature could be linked to the characteristic size of the incoming gust relative to the size of the serration wavelength.
- Identification of a significant interdependence of the angle of attack and the serration wavelength ($z/H \cdot \lambda/C$) with regard to the overall noise reduction capability. This characteristic behavior could be assigned to the three-dimensional effects when the flow is approaching the airfoil and the location of the stagnation points

for the mean flow. The mechanism that causes an increased level of noise radiation at the low serration wavelength has also been suggested.

- An algorithm to achieve the polyoptimum of low-absolute level of noise radiation, as well as high-level of noise reduction has been developed. This will serve as a first step towards practical applications in order to optimize the effective degrees of freedom in the serration design process.

The current model has not yet considered additional influencing parameters such as the serration curvature and the curvature angle of the airfoil leading edge, which could otherwise expand the model to other airfoil geometries. This gap provides an incentive for future work to improve the robustness and fidelity of the current model.

References

[1] Narayanan, S., Chaitanya, P., Haeri, S., Joseph, P., Kim, J. W., and Polacsek, C., "Airfoil noise reductions through leading edge serrations," *Physics of Fluids*; Vol. 27, No. 2, 2015, p. 25109. doi: 10.1063/1.4907798.

[2] Chong, T. P., Vathylakis, A., McEwen, A., Kemsley, F., Muhammad, C., and Siddiqi, S., "Aeroacoustic and Aerodynamic Performances of an Aerofoil Subjected to Sinusoidal Leading Edges," 2015. doi: 10.2514/6.2015-2200.

[3] Chaitanya, P., Narayanan, S., Joseph, P., Vanderwel, C., Kim, J. W., and Ganapathisubramani, B., "Broadband noise reduction through leading edge serrations on realistic aerofoils," 2015. doi: 10.2514/6.2015-2202.

[4] Hersh, A. S., Sodermant, P. T., and Hayden, R. E., "Investigation of Acoustic Effects of Leading-Edge Serrations on Airfoils," *Journal of Aircraft*; Vol. 11, No. 4, 1974, pp. 197–202. doi: 10.2514/3.59219.

[5] Lau, A. S., Haeri, S., and Kim, J. W., "The effect of wavy leading edges on aerofoil–gust interaction noise," *Journal of Sound and Vibration*; Vol. 332, No. 24, 2013, pp. 6234–6253. doi: 10.1016/j.jsv.2013.06.031.

[6] Chen, W., Qiao, W., Wang, L., Tong, F., and Wang, X., "Rod-Airfoil Interaction Noise Reduction Using Leading Edge Serrations," *21st AIAA/CEAS Aeroacoustics Conference*, 2015. doi: 10.2514/6.2015-3264.

[7] Custodio, D., *The Effect of Humpback Whale-like Leading Edge Protuberances on Hydrofoil Performance*, Worcester, USA, December 2007.

[8] Melo De Sousa, J., and Camara, J., "Numerical Study on the Use of a Sinusoidal Leading Edge for Passive Stall Control at Low Reynolds Number," *51st AIAA Aerospace Sciences Meeting*, 2013. doi: 10.2514/6.2013-62.

[9] Gawad, A. F., "Utilization of Whale-Inspired Tubercles as a Control Technique to Improve Airfoil Performance," *Transaction on Control and Mech. Systems*; Vol. 2, No. 5, 2013, pp. 212–218.

[10] Paterson, R. W., and Amiet, R. K., "Acoustic Radiation and Surface Pressure Characteristics of an Airfoil due to Incident Turbulence," United Technologies Research Center for Langley Research Center, NASA CR-2733, September 1976.

[11] Staubs, J. K., *Real Airfoil Effects on Leading Edge Noise*, Blacksburg, USA, May 2008.

[12] Kim, J. W., and Haeri, S., "An advanced synthetic eddy method for the computation of aerofoil–turbulence interaction noise," *Journal of Computational Physics*; Vol. 287, 2015, pp. 1–17. doi: 10.1016/j.jcp.2015.01.039.

[13] Kim, J. W., Haeri, S., and Joseph, P. F., "On the reduction of aerofoil–turbulence interaction noise associated with wavy leading edges," *Journal of Fluid Mechanics*; Vol. 792, 2016, pp. 526–552. doi: 10.1017/jfm.2016.95.

[14] Turner, J., and Kim, J. W., "Towards Understanding Aerofoils with Wavy Leading Edges Interacting with Vortical Disturbances," *22st AIAA/CEAS Aeroacoustics Conference*, 2016. doi: 10.2514/6.2016-2952.

[15] Chaitanya, P., Narayanan, S., Joseph, P., and Kim, J. W., "Leading edge serration geometries for significantly enhanced leading edge noise reductions," *22nd AIAA/CEAS Aeroacoustics Conference*, 2016. doi: 10.2514/6.2016-2736.

[16] Lyu, B., Azarpeyvand, M., and Sinayoko, S., "Noise Prediction for Serrated Leading-edges," *22nd AIAA/CEAS Aeroacoustics Conference*, 2016. doi: 10.2514/6.2016-2740.

[17] Vathylakis, A., Chong, T. P., and Kim, J. H., "Design of a low-noise aeroacoustic wind tunnel facility at Brunel University," *20th AIAA/CEAS Aeroacoustics Conference*, 2016. doi: 10.2514/6.2014-3288.

[18] Laws, E. M., and Livesey, J. L., "Flow Through Screens," *Annual Review of Fluid Mechanics*; Vol. 10, No. 1, 1978, pp. 247–266. doi: 10.1146/annurev.fl.10.010178.001335.

[19] Aufderheide, T., Bode, C., Friedrichs, J., and Kozulovic, D., "The Generation of Higher Levels of Turbulence in in a Low-Speed Cascade Windtunnel by Pressurized Tubes," *11th World Congress on Computational Mechanics*; Vol. 2014, 2014.

[20] Rozenberg, Y., *Modélisation analytique du bruit aérodynamique à largebande des machines tournantes : utilisation de calculs moyennés de mécanique des fuides*, Lyon, 2007.

[21] Amiet, R. K., "Acoustic Radiation from an Airfoil in a Turbulent Stream," *Journal of Sound and Vibration*; Vol. 1975, 41(4), 1975, pp. 407--420.

[22] Gershfeld, J., "Leading Edge Noise from Thick Foils in Turbulent Flows," NSWCCD-72-TR-2003/099, 2003.

[23] Adam, M., *Statistische Versuchsplanung und Auswertung (DoE Design of Experiments)*, University of Applied Sciences Dusseldorf, Germany, 2012.

[24] Clementi, S., Fernandi, M., Baroni, M., Decastri, D., Randazzo, G. M., and Scialpi, F., "Mauro: A Novel Strategy for Optimizing Mixture Properties," *Applied Mathematics*; Vol. 03, No. 10, 2012, pp. 1260–1264. doi: 10.4236/am.2012.330182.

[25] Biedermann, T., *Aerofoil Noise Subjected to Leading Edge Serration*, Düsseldorf, September 2015.

[26] Biedermann, T., Chong, T. P., and Kameier, F., "Statistical-empirical modelling of aerofoil noise subjected to leading edge serrations and aerodynamic identification of noise reduction mechanisms," *22nd AIAA/CEAS Aeroacoustics Conference*, 2016. doi: 10.2514/6.2016-2757.

[27] Kleppmann, W., *Taschenbuch Versuchsplanung. Produkte und Prozesse optimieren*, 5th edn., Hanser, München, 2008.

[28] Siebertz, K., van Bebber, D., and Hochkirchen, T., *Statistische Versuchsplanung*, Springer Berlin Heidelberg, Berlin, Heidelberg, 2010.

[29] Haase, D., *Ein neues Verfahren zur modellbasierten Prozessoptimierung auf der Grundlage der statistischen Versuchsplanung am Beispiel eines Ottomotors mit elektromagnetischer Ventilsteuerung (EMVS)*, Dresden, 2004.

[30] Narayanan, S., Joseph, P., Haeri, S., and Kim, J. W., "Noise Reduction Studies from the Leading Edge of Serrated Flat Plates," *20th AIAA/CEAS Aeroacoustics Conference*, 2014. doi: 10.2514/6.2014-2320.

[31] Hansen, K. L., *Effect of Leading Edge Tubercles on Airfoil Performance*, Adelaide, Australia, July 2012.

[32] Clair, V., Polacsek, C., Le Garrec, T., Reboul, G., Gruber, M., and Joseph, P., "Experimental and Numerical Investigation of Turbulence-Airfoil Noise Reduction Using Wavy Edges," *AIAA Journal*; Vol. 51, No. 11, 2013, pp. 2695–2713. doi: 10.2514/1.J052394.

[33] Gruber, M., *Airfoil noise reduction by edge treatments*, Southampton, UK, February 2012.

[34] Roger, M., Schram, C., and Santana, L. de, "Reduction of Airfoil Turbulence-Impingement Noise by Means of Leading-Edge Serrations and/or Porous Material," *19th AIAA/CEAS Aeroacoustics Conference*, 2013. doi: 10.2514/6.2013-2108.

[35] Polacsek, C., Reboul, G., Clair, V., Le Garrec, T., and Deniau, H., "Turbulence-airfoil interaction noise reduction using wavy leading edge: An experimental and numerical study," *Inter Noise 2011*, 2011.

[36] Oerlemans, S., and Migliore, P., "Aeroacoustic Wind Tunnel Tests of Wind Turbine Airfoils," *10th AIAA/CEAS Aeroacoustics Conference*, 2004. doi: 10.2514/6.2004-3042.

[37] Geyer, T., Sarradj, E., and Giesler, J., "Application of a Beamforming Technique to the Measurement of Airfoil Leading Edge Noise," *Advances in Acoustics and Vibration*; Vol. 2012, No. 3, 2012, pp. 1–16. doi: 10.1155/2012/905461.